

# Optoacoustic entanglement in a continuous Brillouin-active solid state system

Changlong Zhu,<sup>1</sup> Claudiu Genes,<sup>1,2</sup> and Birgit Stiller<sup>1,2,\*</sup>

<sup>1</sup>Max Planck Institute for the Science of Light, Staudtstraße 2, D-91058 Erlangen, Germany

<sup>2</sup>Department of Physics, Friedrich-Alexander-Universität Erlangen-Nürnberg, Staudtstraße 7, D-91058 Erlangen, Germany

(Dated: January 22, 2024)

Entanglement in hybrid quantum systems comprised of fundamentally different degrees of freedom, such as light and mechanics is of interest for a wide range of applications in quantum technologies. Here, we propose to engineer bipartite entanglement between traveling acoustic phonons in a Brillouin active solid state system and the accompanying light wave. The effect is achieved by applying optical pump pulses to state-of-the-art waveguides, exciting a Brillouin Stokes process. This pulsed approach, in a system operating in a regime orthogonal to standard optomechanical setups, allows for the generation of entangled photon-phonon pairs, resilient to thermal fluctuations. We propose an experimental platform where readout of the optoacoustics entanglement is done by the simultaneous detection of Stokes and Anti-Stokes photons in a two-pump configuration. The proposed mechanism presents an important feature in that it does not require initial preparation of the quantum ground state of the phonon mode.

Entanglement between two quantum systems describes a many body quantum state which is not separable and can exhibit quantum correlations even at arbitrarily large distances [1]. It is therefore a resource not only for a plethora of emerging quantum technologies [2–4] such as quantum cryptography [5, 6], quantum teleportation [7, 8], and quantum computation [9], but also offers a tool to deeper study and understand the classical-to-quantum boundary [10]. As many experimental endeavors are easier performed under ambient conditions, it is essential to study possibilities of generating entangled quantum states robust to thermal noise even at room temperature. Cavity optomechanics [11], which provides a platform to explore quantum effects via coupling photons and phonons at the macroscale, has been a hot topic of investigations in terms of generation and measurement of entanglement both in theory [12–15] and experiments [16–18, 56].

Continuum optomechanical systems [20, 21], such as Brillouin-active optical waveguides [22], are a more recent alternative to standard optomechanical cavities, offering a viable platform for the interface between optical photons and continuously accessible groups of acoustic phonons. Such platforms exhibit a powerful performance in quantum information processing with unprecedented acoustic and optical bandwidth compared to cavity optomechanical systems. Especially due to the recent development in nanofabrication, a new breed of chip-based Brillouin-active waveguides with short length ( $\sim$  cm) have been achieved experimentally [23], which enables coherent information transduction [24], information storage [25, 26] and phonon cooling [27, 28]. However, the next logical step after the experimental demonstration of Brillouin cooling [28–30] in continuum optomechanics is the observation of quantum optoacoustical entanglement.

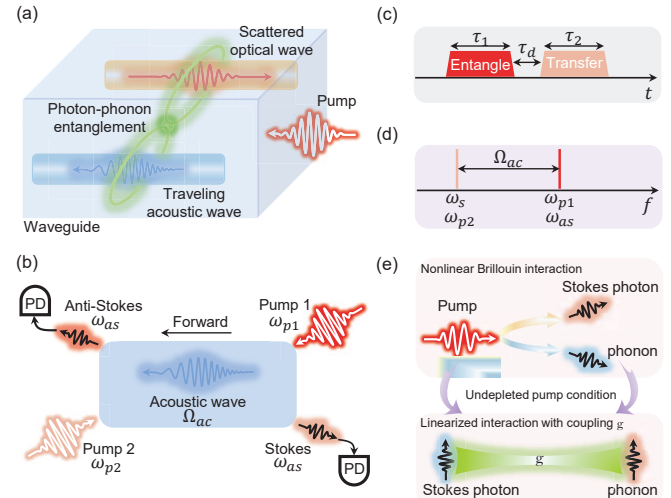


FIG. 1: (a) The Brillouin Stokes scattering implies the down conversion of a pump photon (at  $\omega_p$ ) into a Stokes scattered photon ( $\omega_s$ ) and traveling acoustic phonon (at  $\Omega_{ac}$ ). (b) Protocol for entanglement generation, via pump 1 and detection (at photon-diode detectors PD) via the simultaneous monitoring of both Stokes and Anti-Stokes scattered photons in the presence of pump 2. (c) The timing diagram of the protocol showing the application of an entangling pulse for duration  $\tau_1$  followed by the transfer pulse with duration  $\tau_2$  after the interval  $\tau_d$ . (d) The frequency relations between optical and acoustic waves, i.e.,  $\omega_{p1} - \omega_s = \omega_{as} - \omega_{p2} = \Omega_{ac}$  and  $\omega_{as} = \omega_{p1}$ . (e) In the linearized regime, under the undepleted pump assumption, the nonlinear Brillouin Stokes scattering process can be mapped into a linear Hamiltonian with pump-enhanced coupling strength  $g$ .

In this work, we propose and analyze the feasibility of an experimental scheme (see Fig.1) which enables the generation of bipartite light-matter entanglement in Brillouin-active waveguides. The mechanism is based on a down-conversion like process, where pairs of phonons (frequency  $\Omega_{ac}$ ) and Brillouin Stokes scattered photons

\*Electronic address: birgit.stiller@mpl.mpg.de

(frequency  $\omega_s$ ) are generated from the higher energy pump (with  $\omega_p = \Omega_{\text{ac}} + \omega_s$ ). As opposed to standard optomechanical systems, the acoustic phonons are highly energetic (in the GHz regime) and mechanical losses (rate  $\Gamma$ ) dominate over optical losses (rate  $\gamma$ ). This indicates a departure from the standard continuous operation regime and suggests a pulsed operation scheme, thus circumventing the usual prerequisite of initial quantum ground state cooling [16, 17]. Based on experimental parameters in accordance with state-of-the-art waveguides [23] utilized for experimental proofs of Brillouin cooling [28–30], we present numerical evidence of optoacoustic entanglement in the pulsed regime achieved without the need of employing non-classical quantum states of light [31]. At an ambient phonon occupancy  $n_{\text{th}}$ , for small times  $t < 1/(\Gamma n_{\text{th}})$  an optimized value for the logarithmic negativity [37–39] is obtained in a very simple analytical form reading  $E_{\mathcal{N}}^{\text{max}} \approx -\ln[1 - 2g^2/(\Gamma n_{\text{th}})^2]$ . This entanglement can be detected by homodyne [12] or heterodyne detection [16] of both Stokes photons and anti-Stokes photons produced by a second pump [32] (as illustrated in Fig. 1). More specifically, following the application of a forward-propagating pump with pulse duration  $\tau_1$  to stimulate the Brillouin Stokes process, a delayed (delay time  $\tau_d$ ) backward-propagating pulsed pump with duration  $\tau_2$  is applied to stimulate the Brillouin anti-Stokes process and thus convert the state of the acoustic phonons to a second optical pulse of the anti-Stokes output wave. Our analytical results and numerical investigations demonstrate that this entanglement generation can be fully optically monitored with reasonable values at temperatures above the restrictive cryogenic regime.

**Brillouin Stokes scattering in waveguides.**— Let us first briefly introduce the dynamics of a Brillouin Stokes process under the condition of undepleted constant CW pump laser (pump 1) and with the observation that for backward scattering the process is independent of the anti-Stokes process because of the dispersive symmetry breaking [29, 33]. In the undepleted pump regime, the interaction Hamiltonian can be reduced to a linearized optoacoustic exchange between scattered photons and acoustic phonons with an effective pump-enhanced coupling strength  $g$  [20, 27] (illustrated in Fig. 1(e)). Envelope bosonic operators  $a_s$  and  $b_{\text{ac}}$  can be constructed, corresponding to Stokes and acoustic waves [33–35], i.e.,  $a_s = 1/\sqrt{2\pi} \int dk a(k, t) e^{-ikz}$  and  $b_{\text{ac}} = 1/\sqrt{2\pi} \int dk b(k, t) e^{ikz}$ , where  $a(k, t)$  and  $b(k, t)$  denote annihilation operators for the  $k$ -th Stokes photon mode and acoustic phonon mode, respectively. This formulation captures the time evolution of the amplitude for each mode. Moving into the momentum space, the dynamics of the linearized Stokes process can be given

by [36]

$$\begin{aligned} \frac{da}{dt} &= -\left(\frac{\gamma}{2} + i\Delta_a\right)a - igb^\dagger + \sqrt{\gamma}\xi_a, \\ \frac{db}{dt} &= -\left(\frac{\Gamma}{2} + i\Delta_b\right)b - iga^\dagger + \sqrt{\Gamma}\xi_b, \end{aligned} \quad (1)$$

where  $\Delta_a = kv_{\text{opt}}$  ( $\Delta_b = kv_{\text{ac}}$ ) denote the damping rate and wavenumber-induced frequency shift of the Stokes (acoustic) mode, respectively. Here,  $v_{\text{opt}}$  ( $v_{\text{ac}}$ ) is the group velocity of the Stokes (acoustic) wave. We take the effective coupling strength  $g$  real and positive without loss of generality [20]. The quantum noise operators  $\xi_a$  and  $\xi_b$  are assumed to be zero-averaged [11, 27, 33] and to satisfy the following correlation  $\langle \xi_a(t)\xi_a^\dagger(t') \rangle = \delta(t-t')$  (for the optical mode an effective zero temperature bath can be assumed) and  $\langle \xi_b^\dagger(t)\xi_b(t') \rangle = n_{\text{th}}\delta(t-t')$ , where the thermal phonon occupancy at ambient temperature  $T_m$  is given by  $n_{\text{th}} = (e^{\hbar\Omega_{\text{ac}}/k_B T_m} - 1)^{-1}$  ( $k_B$  is the Boltzmann constant).

**Optoacoustic entanglement via Brillouin Stokes interaction**—In order to quantify entanglement we make use of the logarithmic negativity for continuous variables  $E_{\mathcal{N}}$  introduced in Refs. [37–39] and extensively used in Refs. [12, 40–44]. To this end, we introduce position and momentum quadratures  $x_a = (a + a^\dagger)/\sqrt{2}$ ,  $p_a = i(a^\dagger - a)/\sqrt{2}$ ,  $x_b = (b + b^\dagger)/\sqrt{2}$ , and  $p_b = i(b^\dagger - b)/\sqrt{2}$ . The covariance matrix is then computed  $\mathcal{V}_{ij} = (\langle \phi_i(t)\phi_j(t) + \phi_j(t)\phi_i(t) \rangle)/2 - \langle \phi_i(t) \rangle \langle \phi_j(t) \rangle$ , where the indexes  $i$  and  $j$  go over the vector  $\phi^T(t) = (x_a(t), p_a(t), x_b(t), p_b(t))$  which is the vector of continuous variables operators at time  $t$ . The symmetric matrix  $\mathcal{V}$  can be expressed as the  $2 \times 2$  block form

$$\mathcal{V} = \begin{bmatrix} A & C \\ C^T & B \end{bmatrix}. \quad (2)$$

From this, one computes  $E_{\mathcal{N}} = \max[0, -\ln(2\lambda_-)]$  where  $\lambda_-$  is the minimal symplectic eigenvalue of the covariance matrix  $\mathcal{V}$  under a partial transposition [47] and defined as  $\lambda_- \equiv 2^{-1/2} \sqrt{\Sigma(\mathcal{V}) - [\Sigma(\mathcal{V})^2 - 4 \det \mathcal{V}]^{1/2}}$ , with  $\Sigma(\mathcal{V}) \equiv \det A + \det B - 2 \det C$ . As a general criterion for bimodal Gaussian states, entanglement needs the conditions  $E_{\mathcal{N}} > 0$ , which is equivalent to  $\lambda_- < 1/2$ . Notice that in the particular case of a two mode squeezed state, the logarithmic negativity is simply proportional to the squeezing parameter [45, 46].

Numerically and analytically one can start with Eqs. (1) to compute the time evolution of the covariance matrix. We perform numerical simulations with experimentally feasible values of system parameters [23, 29, 48]:  $\Gamma/2\pi = 2$  MHz,  $\gamma/2\pi = 0.1$  MHz,  $\Omega_{\text{ac}}/2\pi = 7.7$  GHz,  $c = 3 \times 10^8$  m/s,  $n_{\text{opt}} = 2.4$  (index of refraction),  $v_{\text{ac}} = 6000$  m/s,  $T_m = 30$  K, and  $\Delta_a = 0.2\Gamma$ . The results are illustrated in Fig. 2(a) for various ratios of  $g/\Gamma$  deep into the strong coupling regime and indicate that a given time window is available for efficient optoacoustic entanglement generation. We assume that the wavenumber-induced frequency shifts of Stokes and acoustic modes

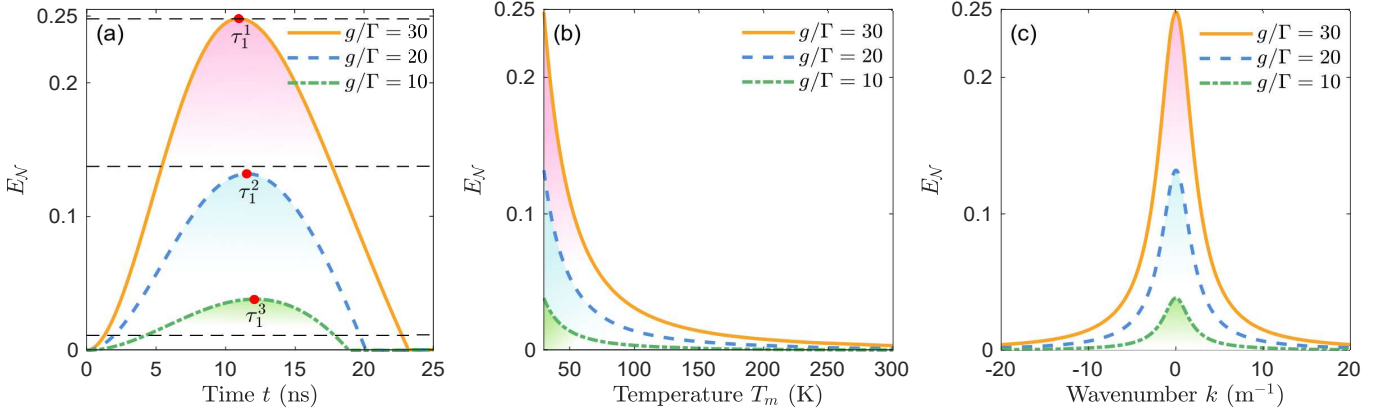


FIG. 2: (a) Time evolution of  $E_N$  at  $T_m = 30$  K for various ratios  $g/\Gamma$ . The red points denote the optimal time for optimal entanglement and black dashed lines correspond to the maximum value of  $E_N$  evaluated by the analytical expression. (b) Variation of  $E_N$  versus  $T_m$  for various ratios  $g/\Gamma$ . (c) Continuum optoacoustic entanglement versus the wavenumber  $k$  in the strong coupling regime at temperature of 30 K.

are within the linewidth of the acoustic mode ( $\Delta_{a,b} < \Gamma$ ), where  $\Delta_a \gg \Delta_b$  since  $v_{\text{opt}} = c/n_{\text{opt}} \gg v_{\text{ac}}$ . The Stokes mode is assumed to be initially in the vacuum state while a thermal state with phonon occupation  $n_0 = n_{\text{th}} \gg 1$  is assumed for the acoustic mode. Under such conditions, a crude approximation for the minimal symplectic eigenvalue  $\lambda_-$  at a high environment temperature is given by the following expression

$$\lambda_- \approx \frac{1}{2} \left[ 1 - 2g^2 t^2 + \frac{2}{3} g^2 (\Gamma n_{\text{th}}) t^3 \right]. \quad (3)$$

A better analytical fit to the exact behavior can be obtained, as listed in the Appendix, albeit in a quite cumbersome form. However, the simplified expression above suffices to understand the mechanisms leading to the generation and suppression of entanglement. While the initial beam splitter exchange can lead to the generation of entanglement by reducing the symplectic eigenvalue below 1/2, at a rate indicated by  $g$ , the environmental induced decoherence rate  $A_{\text{heat}} = \Gamma n_{\text{th}}$  acts in the opposite fashion. The pulse duration that leads to optimal entanglement is found to be on the order of  $A_{\text{heat}}^{-1}$  and the maximally achievable value of the logarithmic negativity can be estimated by

$$E_N^{\text{max}} \approx -\ln \left[ 1 - 2 \left( \frac{g}{A_{\text{heat}}} \right)^2 \right]. \quad (4)$$

The result shows that a necessary condition for such a pulsed scheme to generate considerable entanglement is that the coupling strength overcomes the thermal reheating rate: this is validated by numerical simulations shown in Fig. 2(a). The robustness of such optoacoustic entanglement with respect to environment temperature is presented in Fig. 2(b) showing that high values of optoacoustic entanglement, comparable to other recent results [49–51], can be achieved at a temperature of tens of Kelvins. For example, using the setup of Ref [29], for

a waveguide with the length  $L = 0.5$  m and Brillouin gain  $G_B = 300$  m\$^{-1}\$W\$^{-1}\$, it should be possible to create entangled photon-phonon pairs with  $E_N = 0.3$  at a temperature of 30 K by utilizing a pulsed pump with duration of 11 ns and peak power of 0.5 W.

It should be noted that we only consider the case with a specific wavenumber  $k$  in the above discussion. However, the optical and acoustic waves provide groups of photons and phonons in a continuous optomechanical system [32–36]. Therefore, the system has the capability of producing optoacoustic entanglement over a wide bandwidth of Stokes photons and acoustic phonons. This is illustrated in Fig. 2(c) which shows that the negativity  $E_N$  can achieve considerable values over a large interval of wavenumbers  $k$ , indicating high degree of entanglement over accessible groups of photons and phonons in Brillouin-active waveguides at high environmental temperatures, which is a crucial aspects for a broad range of applications, such as quantum computing [52], quantum communication [53], and sensing [54].

**Optical readout of entanglement** — Although the detection of the optical Stokes field can be directly performed by an optical heterodyne [15, 55] or homodyne measurements [12], direct access to the quantum state of the acoustic field is not easily experimentally achievable. This difficulty can be overcome by transducing the mechanical quantum state into the quantum state of an auxiliary optical mode, followed by standard homodyne detection on such mode. To this end, we propose to employ an additional backward-propagating pump, delayed by time  $\tau_d$ , as shown in Figs. 1(b) and (c). This maps the phonon state into anti-Stokes photons through Brillouin anti-Stokes scattering [32]. In the undepleted pump regime, this process can be treated as a beam-splitter interaction. Such an interaction would lead to a full quantum state swap between the two modes; the additional

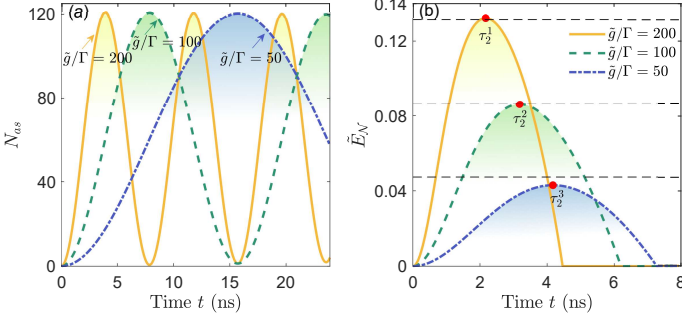


FIG. 3: (a) Time evolution of the anti-Stokes photon occupation  $n_{as}(t)$  in the strong coupling regime at 30 K for various ratios  $\tilde{g}/\Gamma$  during the optical readout process ( $t \in [\tau_1 + \tau_d, \tau_1 + \tau_d + \tau_2]$ ). (b) Corresponding bipartite entanglement between optical modes, where red points denote the optimal time for optimal entanglement and black dashed lines correspond to the maximum value of  $\tilde{E}_N$  evaluated by the fully analytical expression. The coupling strength in the entanglement process is fixed to  $g/\Gamma = 30$ .

presence of decoherence mechanisms simply degrades the fidelity of the swapping process thus requiring finite and quick swap pulses. In terms of quantum Langevin equations this can be cast as

$$\begin{aligned} \frac{d\tilde{a}}{dt} &= -\left(\frac{\gamma}{2} + i\Delta_{\tilde{a}}\right)\tilde{a} - i\tilde{g}b + \sqrt{\gamma}\xi_{\tilde{a}}, \\ \frac{db}{dt} &= -\left(\frac{\Gamma}{2} + i\Delta_b\right)b - i\tilde{g}\tilde{a} + \sqrt{\Gamma}\xi_b, \end{aligned} \quad (5)$$

where  $\tilde{a}$  is the bosonic operator referring at the anti-Stokes mode and we assumed that its loss rate is the same as the one of the Stokes mode  $\gamma$ . Notice that  $\tilde{g}$  denotes the effective coupling strength between the anti-Stokes photons and acoustic phonons. The swapping dynamics can be simply understood from the analytical expression of the number of successfully transferred anti-Stokes quanta. In the strong coupling regime, to a good approximation, this is given by  $e^{-(\gamma+\Gamma)t/2}(1 - \cos 2\tilde{g}t)n_b/2$ , where  $t > 0$  is the time counter during the readout pulse while  $n_b$  corresponds to the phonon number at the beginning of swapping time  $\tau_1 + \tau_d$ . The result shows that an optimal swap is realized at  $t = \pi/(2\tilde{g})$  and affected by the exponential process stemming from optical and phonon decoherence. The time evolution of  $n_{as}(t)$  for various coupling strengths  $\tilde{g}$  is illustrated in Fig. 3(a).

Let us now move on onto the characterization of the observable entanglement between the Stokes and anti-Stokes modes. To this end we solve Eqs. (5) both analytically and numerically for the all optical logarithmic negativity  $\tilde{E}_N$ . After some approximations, a simplified expression of the minimal symplectic eigenvalue  $\lambda_-$  can be casted in the following form

$$\tilde{\lambda}_- \approx \frac{1}{2} \left[ 1 - \eta^2 t^2 + \frac{2}{3} \tilde{g}^2 (\Gamma n_{th}) t^3 \right], \quad (6)$$

which resembles the solution obtained for the acoustic entanglement in Eq. (3) up to third order in  $t$  with an

entanglement generation coefficient  $\eta$  and the decoherence term identical as previously derived. The analytical expression for the entanglement readout rate is

$$\eta^2 = \frac{\tilde{g}^2 (\mathcal{C}_{ns}^2 - 4n_b n_s)}{1 + 2n_s}, \quad (7)$$

with notations  $n_s$  and  $\mathcal{C}_{ns}$  standing for the Stokes photon occupancy and cross-correlation between Stokes photons and acoustic phonons at time  $\tau_1 + \tau_d$  (for more details see Appendix). The solution is remarkably similar to the one in Eq. (3) with the striking difference that the entanglement readout rate depends on the produced entanglement in the write-in part. This can be immediately observed in the expression  $\mathcal{C}_{ns}^2 - 4n_b n_s$  indicating that cross-correlations are needed in order to swap entanglement. As a simple intuitive check, higher temperatures automatically reduce the swapping rate, as the product  $n_b n_s$  increases, up to the point  $\eta$  becomes negative and entanglement readout is no longer possible.

Numerical simulations are illustrated in Fig. 3(b) for various ratios of  $\tilde{g}/\Gamma$ , where the red points correspond to the optimal pulse duration  $\tau_2$  for various  $\tilde{g}$ , respectively. At an environmental temperature around 30 K, the thermal noise is considerable and needs a fast readout time as shown in Fig. 3(b). Realistically, this can be obtained in a pulsed scheme where the entangling pump duration of 11 ns and peak power of 0.5 W is followed by a counter-propagating pump with duration of 3 ns and peak power of 5 W after 0.1 ns delay. We assume a waveguide with the length  $L = 0.5$  m and Brillouin gain  $G_B = 300 \text{ m}^{-1}\text{W}^{-1}$  as achieved in Ref. [29]. For an environmental temperature of 30 K, the acoustic entanglement of peak value  $\tilde{E}_N = 0.3$  will be transduced in an photon-photon entanglement of peak value  $\tilde{E}_N = 0.1$ .

**Conclusions and outlook**— We have shown that optoacoustic entanglement in continuous media, over groups of photons and phonons modes can be achieved through the non-linear optical process of Brillouin scattering. As opposed to standard optomechanics, characterized by extremely high mechanical Q resonators and by operation under steady state conditions, the large mechanical loss characterizing such setups imply operation in the pulsed regime. This presents itself as an advantage, as the possibility of reaching strong phonon-photon coupling allows for the quick generation of entanglement, even in the presence of strong reheating rates. Our estimates show that, utilizing state-of-the-art waveguides where continuous optomechanical cooling has been proved. [29], the generated optoacoustic entanglement can survive in thermal environments far from the exclusive cryogenic requirements. Moreover, quantum ground state cooling of the acoustic mode in this case is not a prerequisite. The generated entanglement bimodal optoacoustic entanglement can be read out by optical detection means, namely by homodyne monitoring of both Stokes and anti-Stokes photons stemming from two different pumps which share the same propagating acoustic mode. The fact that the system operates

over a large bandwidth of both optical and acoustic modes brings a new prospect of entanglement with continuum modes with great potential for applications in quantum computation [52], quantum storage [53], quantum metrology [54], quantum teleportation [56], entanglement-assisted quantum communication [57], and the exploration of the boundary between classical and quantum worlds [58].

**Acknowledgements** This work is supported by the Max-Planck-Society through the independent Max Planck Research Groups Scheme and the Deutsche Forschungsgemeinschaft (DFG, German Research Foundation) – Project-ID 429529648 – TRR 306 QuCoLiMa (“Quantum Cooperativity of Light and Matter”).

---

[1] A. Einstein, B. Podolsky, and N. Rosen, Can Quantum-Mechanical Description of Physical Reality Be Considered Complete? *Phys. Rev.* **47**, 777 (1935).

[2] D. Bouwmeester, A. Ekert, and A. Zeilinger, *The Physics of Quantum Information* (Springer, Berlin, 2000).

[3] S. L. Braunstein and P. Van Loock, Quantum information with continuous variables, *Rev. Mod. Phys.* **77**, 513 (2005).

[4] R. Horodecki, P. Horodecki, M. Horodecki, and K. Horodecki, Quantum entanglement, *Rev. Mod. Phys.* **81**, 865 (2009).

[5] A. K. Ekert, Quantum Cryptography Based on Bell’s Theorem, *Phys. Rev. Lett.* **67**, 661 (1991).

[6] T. Jennewein, C. Simon, G. Weihs, H. Weinfurter, and A. Zeilinger, Quantum Cryptography with Entangled Photons, *Phys. Rev. Lett.* **84**, 4729 (2000).

[7] C. H. Bennett, G. Brassard, C. Crépeau, R. Jozsa, A. Peres, and W. K. Wootters, Teleporting an unknown quantum state via dual classical and Einstein-Podolsky-Rosen channels, *Phys. Rev. Lett.* **70**, 1895 (1993).

[8] S. G. Hofer, W. Wieczorek, M. Aspelmeyer, and K. Hammerer, Quantum entanglement and teleportation in pulsed cavity optomechanics, *Phys. Rev. A* **84**, 052327 (2011).

[9] D. Gottesman and I. L. Chuang, Demonstrating the viability of universal quantum computation using teleportation and single-qubit operations, *Nature* **402**, 390 (1999).

[10] A. J. Leggett, Testing the limits of quantum mechanics: motivation, state of play, prospects, *J. Phys. Condens. Matter* **14**, R415 (2002).

[11] M. Aspelmeyer, T. J. Kippenberg, and F. Marquardt, Cavity optomechanics, *Rev. Mod. Phys.* **86**, 1391 (2014).

[12] D. Vitali, S. Gigan, A. Ferreira, H. R. Böhm, P. Tombesi, A. Guerreiro, V. Vedral, A. Zeilinger, and M. Aspelmeyer, Optomechanical Entanglement between a Movable Mirror and a Cavity Field, *Phys. Rev. Lett.* **98**, 030405 (2007).

[13] M. Paternostro, D. Vitali, S. Gigan, M. S. Kim, C. Brukner, J. Eisert, and M. Aspelmeyer, Creating and Probing Multipartite Macroscopic Entanglement with Light, *Phys. Rev. Lett.* **99**, 250401 (2007).

[14] C. Genes, A. Mari, P. Tombesi, and D. Vitali, Robust entanglement of a micromechanical resonator with output optical fields, *Phys. Rev. A* **78**, 032316 (2008).

[15] A. K. Sarma, S. Chakraborty, and S. Kalita, Continuous variable quantum entanglement in optomechanical systems: A short review, *AVS Quant. Sci.* **3**, 015901 (2021).

[16] T. A. Palomaki, J. D. Teufel, R. W. Simmonds, and K. W. Lehnert, Entangling Mechanical Motion with Microwave Fields, *Science* **342**, 710 (2013).

[17] C. F. Ockeloen-Korppi, E. Damskägg, J.-M. Pirkkalainen, M. Asjad, A. A. Clerk, F. Massel, M. J. Woolley, and M. A. Sillanpää, Stabilized entanglement of massive mechanical oscillators, *Nature (London)* **556**, 478 (2018).

[18] I. Marinković, A. Wallucks, R. Riedinger, S. Hong, M. Aspelmeyer, and Simon Gröblacher, Optomechanical Bell Test, *Phys. Rev. Lett.* **121**, 220404 (2018).

[19] S. Barzanjeh, E. S. Redchenko, M. Peruzzo, M. Wulf, D. P. Lewis, G. Arnold, and J. M. Fink, Stationary entangled radiation from micromechanical motion, *Nature (London)* **570**, 480 (2019).

[20] R. Van Laer, R. Baets, and D. Van Thourhout, Unifying Brillouin scattering and cavity optomechanics, *Phys. Rev. A* **93**, 053828 (2016).

[21] P. Rakich and F. Marquardt, Quantum theory of continuum optomechanics, *New J. Phys.* **20**, 045005 (2018).

[22] C. Wolff, M. J. Steel, B. J. Eggleton, and C. G. Poulton, Stimulated Brillouin scattering in integrated photonic waveguides: Forces, scattering mechanisms, and coupled-mode analysis, *Phys. Rev. A* **92**, 013836 (2015).

[23] B. J. Eggleton, C. G. Poulton, P. T. Rakich, M. J. Steel, and G. Bahl, Brillouin integrated photonics, *Nat. Photonics* **13**, 664 (2019).

[24] H. Shin, J. A. Cox, R. Jarecki, A. Starbuck, Z. Wang, and P. T. Rakich, Control of coherent information via on-chip photonic-phononic emitter-receivers, *Nat. Commun.* **6**, 6427 (2015).

[25] M. Merklein, B. Stiller, K. Vu, S. J. Madden, and B. J. Eggleton, A chip-integrated coherent photonic-phononic memory, *Nat. Commun.* **8**, 574 (2017).

[26] B. Stiller, M. Merklein, C. Wolff, K. Vu, P. Ma, S. J. Madden, and B. J. Eggleton, Coherently refreshing hypersonic phonons for light storage, *Optica* **7**, 492 (2020).

[27] Y.-C. Chen, S. Kim, and G. Bahl, Brillouin cooling in a linear waveguide, *New J. Phys.* **18**, 115004 (2016).

[28] N. T. Otterstrom, R. O. Behunin, E. A. Kittlaus, and P. T. Rakich, Optomechanical Cooling in a Continuous System, *Phys. Rev. X* **8**, 041034 (2018).

[29] L. B. Martinez, P. Wiedemann, C. L. Zhu, A. Geilen, and B. Stiller, Optoacoustic cooling of traveling hypersound waves, *Phys. Rev. Lett.* **132**, 023603 (2024).

[30] J. N. Johnson, D. R. Haverkamp, Y.-H. Ou, K. Kieu, N. T. Otterstrom, P. T. Rakich, and R. O. Behunin, Laser cooling of traveling wave phonons in an optical fiber, *arXiv:2305.11796*.

[31] P. Sekatski, M. Aspelmeyer, and N. Sangouard, Macroscopic Optomechanical from Displaced Single-Photon Entanglement, *Phys. Rev. Lett.* **112**, 080502 (2014).

[32] J. Y. Zhang, C. L. Zhu, C. Wolff, and B. Stiller, Quantum coherent control in pulsed waveguide optomechanics, *Phys. Rev. Research* **5**, 013010 (2023).

[33] P. Kharel, R. O. Behunin, W. H. Renninger, and P. T. Rakich, Noise and dynamics in forward Brillouin scattering, *Phys. Rev. A* **93**, 063806 (2016).

[34] J. E. Sipe and M. J. Steel, A Hamiltonian treatment of stimulated Brillouin scattering in nanoscale integrated waveguides, *New J. Phys.* **18**, 045004 (2016).

[35] H. Zoubi and K. Hammerer, Optomechanical multimode Hamiltonian for nanophotonic waveguides, *Phys. Rev. A* **94**, 053827 (2016).

[36] C. L. Zhu and B. Stiller, Dynamic Brillouin cooling for continuous optomechanical systems, *Mater. Quantum Technol.* **3**, 015003 (2023).

[37] K. Życzkowski, P. Horodecki, A. Sanpera, and M. Lewenstein, Volume of the set of separable states, *Phys. Rev. A* **58**, 883 (1998).

[38] G. Vidal, R. F. Werner, Computable measure of entanglement, *Phys. Rev. A* **65**, 032314 (2002).

[39] G. Adesso, A. Serafini, and F. Illuminati, Extremal entanglement and mixedness in continuous variable systems, *Phys. Rev. A* **70**, 022318 (2004).

[40] B. Rogers, M. Paternostro, G. M. Palma, and G. De Chiara, Entanglement control in hybrid optomechanical systems, *Phys. Rev. A* **86**, 042323 (2012).

[41] Y. D. Wang and A. A. Clerk, Reservoir-Engineered Entanglement in Optomechanical Systems, *Phys. Rev. Lett.* **110**, 253601 (2013).

[42] L. Tian, Robust Photon Entanglement via Quantum Interference in Optomechanical Interfaces, *Phys. Rev. Lett.* **110**, 233602 (2013).

[43] S. S. Zheng, F. X. Sun, Y. j. Lai, Q. H. Gong, and Q. Y. He, Manipulation and enhancement of asymmetric steering via interference effects induced by closed-loop coupling, *Phys. Rev. A* **99**, 022335 (2019).

[44] F. X. Sun, S. S. Zheng, Y. Xiao, Q. H. Gong, Q. Y. He, and K. Xia, Remote Generation of Magnon Schrödinger Cat State via Magnon-Photon Entanglement, *Phys. Rev. Lett.* **127**, 087203 (2021).

[45] S. Zippilli and F. Illuminati, Non-Markovian dynamics and steady-state entanglement of cavity arrays in finite-bandwidth squeezed reservoirs, *Phys. Rev. A* **89**, 033803 (2014).

[46] S. Zippilli, G. Di Giuseppe, and D. Vitali, Entanglement and squeezing of continuous-wave stationary light, *New J. Phys.* **17**, 043025 (2015).

[47] S. Pirandola, A. Serafini, and S. Lloyd, Correlation matrices of two-mode bosonic systems, *Phys. Rev. A* **79**, 052327 (2009).

[48] M. Merklein, A. Gasas-Bedoya, D. Marpaung, T. F. S. Büttner, M. Pagani, B. Morrison, I. V. Kabakova, and B. J. Eggleton, Stimulated Brillouin Scattering in Photonic Integrated Circuits: Novel Applications and Devices, *IEEE J. Sel. Top. Quantum Eletron.* **22** (2016).

[49] M. Yu, H. Shen, and J. Li, Magnetostrictively Induced Stationary Entanglement between Two Microwave Fields, *Phys. Rev. Lett.* **124**, 213604 (2020).

[50] Y. F. Jiao, S. D. Zhang, Y. L. Zhang, A. Miranowicz, L. M. Kuang, and H. Jing, Nonreciprocal Optomechanical Entanglement against Backscattering Losses, *Phys. Rev. Lett.* **125**, 143605 (2020).

[51] D. G. Lai, J. Q. Liao, A. Miranowicz, and F. Nori, Noise-Tolerant Optomechanical Entanglement via Synthetic Magnetism, *Phys. Rev. Lett.* **129**, 063602 (2022).

[52] U. L. Andersen, J. S. Neergaard-Nielsen, P. van Loock, and A. Furusawa, Hybrid discrete- and continuous-variable quantum information, *Nat. Phys.* **11**, 713 (2015).

[53] E. Saglamyurek, N. Sinclair, J. Jin, J. A. Slater, D. Oblak, F. Bussières, M. George, R. Sohler, and W. Tittel, Broadband waveguide quantum memory for entangled photons, *Nature (London)* **469**, 512 (2011).

[54] Y. Xia, A. R. Agrawal, C. M. Pluchar, A. J. Brady, Z. Liu, Q. Zhuang, D. J. Wilson, and Z. Zhang, Entanglement-enhanced optomechanical sensing, *Nat. Photonics* **17**, 470 (2023).

[55] R. Sahu, L. Qiu, W. Hease, G. Arnold, Y. Minoguchi, P. Rabl, and J. M. Fink, Entangling microwaves with optical light, *Science* **380**, 718 (2023).

[56] S. Barzanjeh, M. Abdi, G. J. Milburn, P. Tombesi, and D. Vitali, Reversible Optical-to-Microwave Quantum Interface, *Phys. Rev. Lett.* **109**, 130503 (2012).

[57] A. Piveteau, J. Pauwels, E. Håkansson, S. Muhammad, M. Bourennane, and A. Tavakoli, Entanglement-assisted quantum communication with simple measurement, *Nat. Commun.* **13**, 7878 (2022).

[58] W. H. Zurek, Decoherence, einselection, and the quantum origins of the classical, *Rev. Mod. Phys.* **75**, 715 (2003).

### Appendix A: Dynamics of Brillouin Stokes scattering with undepleted pump

In a typical Brillouin-active waveguide, the backward Brillouin Stokes scattering provides an optomechanical interaction between a pump field, a scattered optical field at redder Stokes frequency, and an acoustic field. The motion equations of this Brillouin optoacoustic interaction can be given by

$$\begin{aligned}\frac{\partial a_p}{\partial t} + v_{\text{opt}} \frac{\partial a_p}{\partial z} &= -\frac{\gamma}{2} a_p - i g_0 a_s b_{\text{ac}} + \sqrt{\gamma} \xi_p, \\ \frac{\partial a_s}{\partial t} - v_{\text{opt}} \frac{\partial a_s}{\partial z} &= -\frac{\gamma}{2} a_s - i g_0 b_{\text{ac}}^\dagger a_p + \sqrt{\gamma} \xi_s, \\ \frac{\partial b_{\text{ac}}}{\partial t} + v_{\text{ac}} \frac{\partial b_{\text{ac}}}{\partial z} &= -\frac{\Gamma}{2} b_{\text{ac}} - i g_0 a_s^\dagger a_p + \sqrt{\Gamma} \xi_{\text{ac}},\end{aligned}\quad (\text{A1})$$

where  $a_p$ ,  $a_s$ , and  $b_{\text{ac}}$  correspond to the envelope operators of pump field, Stokes field, and acoustic field with carrier frequencies  $\omega_p$ ,  $\omega_s$ ,  $\Omega_{\text{ac}}$ , respectively.  $v_{\text{opt}}$  ( $\gamma$ ) and  $v_{\text{ac}}$  ( $\Gamma$ ) denote group velocities (dissipation rates) of optical and acoustic fields.  $g_0$  quantifies the coupling strength between these three fields at the single quanta level. Without loss of generality, we take  $g_0$  real and positive [20] in the following discussion.  $\xi_p$ ,  $\xi_s$ , and  $\xi_{\text{ac}}$  represent Langevin noises for these three fields, which obey the following statistical properties

$$\begin{aligned}\langle \xi_p(t, z) \rangle &= \langle \xi_s(t, z) \rangle = \langle \xi_{\text{ac}}(t, z) \rangle = 0, \\ \langle \xi_p^\dagger(t_1, z_1) \xi_p(t_2, z_2) \rangle &= \langle \xi_s^\dagger(t_1, z_1) \xi_s(t_2, z_2) \rangle = 0, \\ \langle \xi_{\text{ac}}^\dagger(t_1, z_1) \xi_{\text{ac}}(t_2, z_2) \rangle &= n_{\text{th}} \delta(t_1 - t_2) \delta(z_1 - z_2),\end{aligned}\quad (\text{A2})$$

where  $n_{\text{th}} = 1/(e^{\hbar\Omega_{\text{ac}}/k_B T_m} - 1)$  denotes the thermal phonon occupation of the acoustic field at temperature  $T_m$ . Considering an undepleted pump field, the three-field optoacoustic interaction can be treated as an effective interaction between optical Stokes field and acoustic field with an effective coupling strength. Thus Eq. (A1) can be reduced to

$$\begin{aligned}\frac{\partial a_s}{\partial t} - v_{\text{opt}} \frac{\partial a_s}{\partial z} &= -\frac{\gamma}{2} a_s - i g b_{\text{ac}}^\dagger + \sqrt{\gamma} \xi_s, \\ \frac{\partial b_{\text{ac}}}{\partial t} + v_{\text{ac}} \frac{\partial b_{\text{ac}}}{\partial z} &= -\frac{\Gamma}{2} b_{\text{ac}} - i g a_s^\dagger + \sqrt{\Gamma} \xi_{\text{ac}},\end{aligned}\quad (\text{A3})$$

where  $g = g_0 \sqrt{\langle a_p^\dagger a_p \rangle}$  is the pump-enhanced coupling strength between Stokes photons and acoustic phonons. As  $a_s$  and  $b_{\text{ac}}$  represent envelope operators with continuum modes and can be expressed in the discrete variable representation as follows [33–35]

$$\begin{aligned}a_s(t, z) &= \frac{1}{\sqrt{2\pi}} \int a(t, k) e^{-ikz} dk, \\ b_{\text{ac}}(t, z) &= \frac{1}{\sqrt{2\pi}} \int b(t, k) e^{ikz} dk.\end{aligned}\quad (\text{A4})$$

Substituting the above discrete form of envelope operators into Eq. (A3), the dynamics of the reduced optomechanical interaction can be re-expressed as

$$\begin{aligned}\frac{da(t, k)}{dt} &= -ikv_{\text{opt}} a - \frac{\gamma}{2} a - i g b^\dagger + \sqrt{\gamma} \xi_a(t, k), \\ \frac{db(t, k)}{dt} &= -ikv_{\text{ac}} b - \frac{\Gamma}{2} b - i g a^\dagger + \sqrt{\Gamma} \xi_b(t, k),\end{aligned}\quad (\text{A5})$$

where  $a$  ( $b$ ) represents the annihilation operator for the  $k$ -th Stokes photon (acoustic phonon) mode with wavenumber  $k$ .  $\xi_a(t, k)$  and  $\xi_b(t, k)$  are inverse Fourier transform of Langevin noises  $\xi_s(t, z)$  and  $\xi_{\text{ac}}(t, z)$ , respectively. Thus the dynamics of the reduced Brillouin Stokes process in momentum space can be described as follows

$$\begin{aligned}\frac{da}{dt} &= -\left(\frac{\gamma}{2} + i\Delta_a\right) a - i g b^\dagger + \sqrt{\gamma} \xi_a, \\ \frac{db}{dt} &= -\left(\frac{\Gamma}{2} + i\Delta_b\right) b - i g a^\dagger + \sqrt{\Gamma} \xi_b,\end{aligned}\quad (\text{A6})$$

where  $\Delta_a = kv_{\text{opt}}$  and  $\Delta_b = kv_{\text{ac}}$  denote wavenumber-induced frequency shifts for Stokes and acoustic modes.  $\xi_a$  and  $\xi_b$  are zero-mean quantum Gaussian noises which obey  $\langle \xi_a(t_1)\xi_a^\dagger(t_2) \rangle = \delta(t_1-t_2)$  and  $\langle \xi_b(t_1)\xi_b^\dagger(t_2) \rangle = (1+n_{\text{th}})\delta(t_1-t_2)$ . The analytical solutions of Eq. (A6) can be given by

$$\begin{aligned} a(t) &= (\mu_2 e^{\omega_+ t} - \mu_3 e^{\omega_- t}) a_s(0) + (-e^{\omega_+ t} + e^{\omega_- t}) \mu_1 b^\dagger(0) + \sqrt{\gamma} \int_0^t [\mu_2 e^{\omega_+(t-\tau)} - \mu_3 e^{\omega_-(t-\tau)}] \xi_a(\tau) d\tau \\ &\quad + \sqrt{\Gamma} \mu_1 \int_0^t [-e^{\omega_+(t-\tau)} + e^{\omega_-(t-\tau)}] \xi_b^\dagger(\tau) d\tau, \\ b(t) &= \mu_1^* (e^{\omega_+^* t} - e^{\omega_-^* t}) a^\dagger(0) + (-\mu_3^* e^{\omega_+^* t} + \mu_2^* e^{\omega_-^* t}) b(0) + \sqrt{\gamma} \mu_1^* \int_0^t [e^{\omega_+^*(t-\tau)} - e^{\omega_-^*(t-\tau)}] \xi_a^\dagger(\tau) d\tau \\ &\quad + \sqrt{\Gamma} \int_0^t [-\mu_3^* e^{\omega_+^*(t-\tau)} + \mu_2^* e^{\omega_-^*(t-\tau)}] \xi_b(\tau) d\tau, \end{aligned} \quad (\text{A7})$$

where

$$\begin{aligned} \omega_+ &= -\frac{\gamma + \Gamma}{4} - i\frac{\Delta_a - \Delta_b}{2} - \frac{\sqrt{16g^2 + [(\Gamma - \gamma) + 2i(\Delta_a + \Delta_b)]^2}}{4}, \\ \omega_- &= -\frac{\gamma + \Gamma}{4} - i\frac{\Delta_a - \Delta_b}{2} + \frac{\sqrt{16g^2 + [(\Gamma - \gamma) + 2i(\Delta_a + \Delta_b)]^2}}{4}, \\ \tau_+ &= -\frac{2(\Delta_a + \Delta_b) + i(\Gamma - \gamma)}{4g} + i\frac{\sqrt{16g^2 + [(\Gamma - \gamma) + 2i(\Delta_a + \Delta_b)]^2}}{4g}, \\ \tau_- &= -\frac{2(\Delta_a + \Delta_b) + i(\Gamma - \gamma)}{4g} - i\frac{\sqrt{16g^2 + [(\Gamma - \gamma) + 2i(\Delta_a + \Delta_b)]^2}}{4g}, \end{aligned} \quad (\text{A8})$$

and

$$\mu_1 = \frac{1}{\tau_+ - \tau_-}, \quad \mu_2 = \frac{\tau_+}{\tau_+ - \tau_-}, \quad \mu_3 = \frac{\tau_-}{\tau_+ - \tau_-} \quad (\text{A9})$$

## Appendix B: Optoacoustic entanglement generated by Brillouin Stokes process

In the above discussion, we analyzed the dynamics of Brillouin Stokes process and obtained the analytical solutions of the generated Stokes photons and acoustic phonons. In order to quantify the inseparability between Stokes photons and acoustic phonons, we consider the logarithmic negativity  $E_N$  [37–39].

We define the quadrature phase operators of Stokes photons and acoustic phonons as follows

$$\begin{aligned} x_1 &= \frac{a + a^\dagger}{\sqrt{2}}, \quad p_1 = \frac{a - a^\dagger}{i\sqrt{2}}, \\ x_2 &= \frac{b + b^\dagger}{\sqrt{2}}, \quad p_2 = \frac{b - b^\dagger}{i\sqrt{2}}. \end{aligned} \quad (\text{B1})$$

By applying the following variable transformation

$$\begin{bmatrix} \phi_1 \\ \phi_2 \\ \phi_3 \\ \phi_4 \end{bmatrix} = \begin{bmatrix} x_1 \\ p_1 \\ x_2 \\ p_2 \end{bmatrix}, \quad (\text{B2})$$

the covariance matrix  $\mathcal{V}$  which evaluates the correlation between Stokes photons and acoustic phonons can be expressed as

$$\mathcal{V}_{ij} = \frac{\langle \phi_i(t)\phi_j(t) \rangle + \langle \phi_j(t)\phi_i(t) \rangle}{2} - \langle \phi_i(t) \rangle \langle \phi_j(t) \rangle. \quad (\text{B3})$$

This symmetric covariance matrix  $\mathcal{V}$  can be also re-written in the  $2 \times 2$  block form

$$\mathcal{V} = \begin{bmatrix} A & C \\ C^T & B \end{bmatrix}. \quad (\text{B4})$$

We define the logarithmic negativity  $E_{\mathcal{N}}$  [38, 39] as follows

$$E_{\mathcal{N}} = \max [0, -\ln 2\lambda_-], \quad (\text{B5})$$

where  $\lambda_-$  denotes the minimal symplectic eigenvalue of the matrix, which is achieved by applying a partial transposition to the covariance matrix [47] and can be calculated as follows

$$\lambda_- \equiv \frac{\sqrt{\Sigma(\mathcal{V}) - \sqrt{\Sigma(\mathcal{V})^2 - 4 \det \mathcal{V}}}}{\sqrt{2}}, \quad (\text{B6})$$

with

$$\Sigma(\mathcal{V}) = \det A + \det B - 2 \det C. \quad (\text{B7})$$

We assume that there is no optical Stokes field at the beginning, i.e., the vacuum state, and the initial state of the acoustic field is the thermal state with phonon occupation  $n_0 = n_{\text{th}}$ . Substituting Eq. (A7) into Eq. (B3) and combining with the initial states of optical and acoustic modes and properties of Langevin noises  $\xi_{a,b}$ , the ten independent elements of covariance matrix  $\mathcal{V}$  can be expressed as

$$\begin{aligned} \mathcal{V}_{11} = & \frac{|\mu_2 e^{\omega_+ t} - \mu_3 e^{\omega_- t}|^2}{2} + \frac{|-e^{\omega_+ t} + e^{\omega_- t}|^2}{2} |\mu_1|^2 (2n_0 + 1) \\ & + \frac{\gamma |\mu_2|^2 + \Gamma(2n_{\text{th}} + 1) |\mu_1|^2}{2\alpha_1} (e^{\alpha_1 t} - 1) - \frac{\gamma \mu_2 \mu_3^* + \Gamma(2n_{\text{th}} + 1) |\mu_1|^2}{2\alpha_2} (e^{\alpha_2 t} - 1) \\ & - \frac{\gamma \mu_3 \mu_2^* + \Gamma(2n_{\text{th}} + 1) |\mu_1|^2}{2\alpha_3} (e^{\alpha_3 t} - 1) + \frac{\gamma |\mu_3|^2 + \Gamma(2n_{\text{th}} + 1) |\mu_1|^2}{2\alpha_4} (e^{\alpha_4 t} - 1), \end{aligned} \quad (17-1)$$

$$\mathcal{V}_{12} = 0, \quad (17-2)$$

$$\begin{aligned} \mathcal{V}_{13} = & \frac{(e^{\omega_+ t} - e^{\omega_- t})(\mu_2^* e^{\omega_+^* t} - \mu_3^* e^{\omega_-^* t})}{4} \mu_1 + \frac{(\mu_2 e^{\omega_+ t} - \mu_3 e^{\omega_- t})(e^{\omega_+^* t} - e^{\omega_-^* t})}{4} \mu_1^* \\ & + \frac{(\mu_1 \mu_3^* + \mu_3 \mu_1^*) e^{\alpha_1 t} - (\mu_1 \mu_2^* + \mu_3 \mu_1^*) e^{\alpha_2 t} - (\mu_3^* \mu_1 + \mu_2 \mu_1^*) e^{\alpha_3 t} + (\mu_1 \mu_2^* + \mu_2 \mu_1^*) e^{\alpha_4 t}}{4} (1 + 2n_0) \\ & + \frac{\gamma (\mu_1 \mu_2^* + \mu_1^* \mu_2) + \Gamma(1 + 2n_{\text{th}}) (\mu_1 \mu_3^* + \mu_3 \mu_1^*)}{4\alpha_1} (e^{\alpha_1 t} - 1) \\ & - \frac{\gamma (\mu_1 \mu_3^* + \mu_1^* \mu_3) + \Gamma(1 + 2n_{\text{th}}) (\mu_1 \mu_2^* + \mu_3 \mu_1^*)}{4\alpha_2} (e^{\alpha_2 t} - 1) \\ & - \frac{\gamma (\mu_1 \mu_2^* + \mu_1^* \mu_2) + \Gamma(1 + 2n_{\text{th}}) (\mu_1 \mu_3^* + \mu_2 \mu_1^*)}{4\alpha_3} (e^{\alpha_3 t} - 1) \\ & + \frac{\gamma (\mu_1 \mu_3^* + \mu_1^* \mu_3) + \Gamma(1 + 2n_{\text{th}}) (\mu_1 \mu_2^* + \mu_2 \mu_1^*)}{4\alpha_4} (e^{\alpha_4 t} - 1), \end{aligned} \quad (17-3)$$

$$\begin{aligned}
\mathcal{V}_{14} = & i \frac{(\mu_2^* \mu_1 - \mu_2 \mu_1^*) e^{\alpha_1 t} + (\mu_1^* \mu_2 - \mu_3^* \mu_1) e^{\alpha_2 t} + (\mu_1^* \mu_3 - \mu_2^* \mu_1) e^{\alpha_3 t} + (\mu_3^* \mu_1 - \mu_1^* \mu_3) e^{\alpha_4 t}}{4} \\
& + i \frac{(\mu_3 \mu_1^* - \mu_1 \mu_3^*) e^{\alpha_1 t} + (\mu_1 \mu_2^* - \mu_3 \mu_1^*) e^{\alpha_2 t} + (\mu_1 \mu_3^* - \mu_2 \mu_1^*) e^{\alpha_3 t} + (\mu_2 \mu_1^* - \mu_1 \mu_2^*) e^{\alpha_4 t}}{4} (1 + 2n_0) \\
& + i \frac{\gamma(\mu_1 \mu_2^* - \mu_1^* \mu_2) + \Gamma(1 + 2n_{\text{th}})(\mu_3 \mu_1^* - \mu_1 \mu_3^*)}{4\alpha_1} (e^{\alpha_1 t} - 1) \\
& + i \frac{\gamma(\mu_1^* \mu_2 - \mu_1 \mu_3^*) + \Gamma(1 + 2n_{\text{th}})(\mu_1 \mu_2^* - \mu_1^* \mu_3)}{4\alpha_2} (e^{\alpha_2 t} - 1) \\
& + i \frac{\gamma(\mu_1^* \mu_3 - \mu_1 \mu_2^*) + \Gamma(1 + 2n_{\text{th}})(\mu_1 \mu_3^* - \mu_1^* \mu_2)}{4\alpha_3} (e^{\alpha_3 t} - 1) \\
& + i \frac{\gamma(\mu_1 \mu_3^* - \mu_3 \mu_1^*) + \Gamma(1 + 2n_{\text{th}})(\mu_2 \mu_1^* - \mu_1 \mu_2^*)}{4\alpha_4} (e^{\alpha_4 t} - 1), \tag{17-4}
\end{aligned}$$

$$\mathcal{V}_{22} = \mathcal{V}_{11}, \tag{17-5}$$

$$\mathcal{V}_{23} = \mathcal{V}_{14}, \tag{17-6}$$

$$\mathcal{V}_{24} = -\mathcal{V}_{13}, \tag{17-7}$$

$$\begin{aligned}
\mathcal{V}_{33} = & \frac{e^{\omega+t} - e^{\omega-t}}{2} |\mu_1|^2 + \frac{|\mu_3|^2 e^{\alpha_1 t} - \mu_3 \mu_2^* e^{\alpha_2 t} - \mu_2 \mu_3^* e^{\alpha_3 t} + |\mu_2|^2 e^{\alpha_4 t}}{2} (1 + 2n_0) \\
& + \frac{\gamma |\mu_1|^2 + \Gamma(1 + 2n_{\text{th}}) |\mu_3|^2}{2\alpha_1} (e^{\alpha_1 t} - 1) - \frac{\gamma |\mu_1|^2 + \Gamma(1 + 2n_{\text{th}}) \mu_3 \mu_2^*}{2\alpha_2} (e^{\alpha_2 t} - 1) \\
& - \frac{\gamma |\mu_1|^2 + \Gamma(1 + 2n_{\text{th}}) \mu_2 \mu_3^*}{2\alpha_3} (e^{\alpha_3 t} - 1) + \frac{\gamma |\mu_1|^2 + \Gamma(1 + 2n_{\text{th}}) |\mu_2|^2}{2\alpha_4} (e^{\alpha_4 t} - 1) \tag{17-8}
\end{aligned}$$

$$\mathcal{V}_{34} = 0, \tag{17-9}$$

$$\mathcal{V}_{44} = \mathcal{V}_{33}, \tag{17-10}$$

(B8)

where

$$\begin{aligned}
\alpha_1 &= \omega_+ + \omega_+^*, \quad \alpha_2 = \omega_+ + \omega_-^*, \\
\alpha_3 &= \omega_- + \omega_-^*, \quad \alpha_4 = \omega_- + \omega_-^*.
\end{aligned}$$

Substituting above solutions into  $\Sigma(\mathcal{V})$  and  $\det \mathcal{V}$ , we have

$$\begin{aligned}
\Sigma(\mathcal{V}) &= \mathcal{V}_{11}^2 + \mathcal{V}_{33}^2 + 2(\mathcal{V}_{13}^2 + \mathcal{V}_{14}^2), \\
\det \mathcal{V} &= (\mathcal{V}_{13}^2 + \mathcal{V}_{14}^2 - \mathcal{V}_{11} \mathcal{V}_{33})^2. \tag{B9}
\end{aligned}$$

We consider the strong coupling regime, i.e.,  $g \gg \gamma, \Gamma$  and assume that the wavenumber-induced frequency shifts  $\Delta_{a,b}$  are within the linewidth of the acoustic field, i.e.,  $\Delta_{a,b} < \Gamma$ . For the backward Brillouin scattering in a typical waveguide, the optical loss is far smaller than the acoustic loss, i.e.,  $\gamma \ll \Gamma$ . Under these conditions, we have  $\det \mathcal{V}/(\Sigma(\mathcal{V}))^2 \ll 1$  and thus can approximately calculate  $\lambda_-$  as follows

$$\begin{aligned}
\lambda_- &= \sqrt{\frac{\Sigma(\mathcal{V}) - \sqrt{(\Sigma(\mathcal{V}))^2 - 4 \det \mathcal{V}}}{2}} \\
&= \sqrt{\frac{\Sigma(\mathcal{V}) - \Sigma(\mathcal{V}) \sqrt{1 - \frac{4 \det \mathcal{V}}{(\Sigma(\mathcal{V}))^2}}}{2}} \\
&\approx \sqrt{\frac{\det \mathcal{V}}{\Sigma(\mathcal{V})}} \\
&\approx \frac{|\mathcal{V}_{13}^2 + \mathcal{V}_{14}^2 - \mathcal{V}_{11} \mathcal{V}_{33}|}{\sqrt{\mathcal{V}_{11}^2 + \mathcal{V}_{33}^2 + 2(\mathcal{V}_{13}^2 + \mathcal{V}_{14}^2)}} \\
&\approx \frac{|\mathcal{V}_{14}^2 - \mathcal{V}_{11} \mathcal{V}_{33}|}{\sqrt{\mathcal{V}_{11}^2 + \mathcal{V}_{33}^2 + 2\mathcal{V}_{14}^2}} \\
&\approx \frac{|\mathcal{V}_{14}^2 \mathcal{V}_{33} - \mathcal{V}_{11} \mathcal{V}_{33}^2|}{\mathcal{V}_{33}^2 + \mathcal{V}_{14}^2}, \tag{B10}
\end{aligned}$$

i.e.,

$$\lambda_- \approx \frac{|\mathcal{V}_{14}^2 \mathcal{V}_{33} - \mathcal{V}_{11} \mathcal{V}_{33}^2|}{\mathcal{V}_{33}^2 + \mathcal{V}_{14}^2}. \quad (\text{B11})$$

The approximated elements of  $\mathcal{V}_{33}$ ,  $\mathcal{V}_{14}$ , and  $\mathcal{V}_{11}$  can be given by

$$\begin{aligned} \mathcal{V}_{33} &\approx \eta_{11} e^{\alpha_1 t} + \eta_{12} e^{\alpha_4 t} + \eta_{13} e^{-\frac{\gamma+\Gamma}{2} t} + \eta_{14}, \\ \mathcal{V}_{14} &\approx \eta_{21} e^{\alpha_1 t} + \eta_{22} e^{\alpha_4 t} + \eta_{23} e^{-\frac{\gamma+\Gamma}{2} t} + \eta_{24}, \\ \mathcal{V}_{11} &\approx \eta_{31} e^{\alpha_1 t} + \eta_{32} e^{\alpha_4 t} + \eta_{33} e^{-\frac{\gamma+\Gamma}{2} t} + \eta_{34}, \end{aligned} \quad (\text{B12})$$

where the coefficients  $\eta_{ij}$  can be calculated as

$$\begin{aligned} \eta_{11} &= \frac{g^2(1+n_{\text{th}})}{4\Delta} \left[ 1 + \frac{\Gamma - \gamma}{2g} - \frac{2\Gamma + \frac{\Gamma(\Gamma-\gamma)}{g}}{4\sqrt{\Delta} + (\gamma + \Gamma)} \right], \\ \eta_{12} &= \frac{g^2}{8\Delta} \left[ 1 + \frac{(g - \frac{\Gamma-\gamma}{4})^2 + (\frac{\Gamma-\gamma}{4})^2}{g^2} (1 + 2n_{\text{th}}) + 2 \frac{(g - \frac{\Gamma-\gamma}{4})^2 + (\frac{\Gamma-\gamma}{4})^2}{g^2 (4\sqrt{\Delta} - (\gamma + \Gamma))} \Gamma (1 + 2n_{\text{th}}) \right], \\ \eta_{13} &= -\frac{\Gamma + (\Gamma - \gamma)n_{\text{th}}}{2\Delta(\gamma + \Gamma)} g^2, \\ \eta_{14} &= (1 + 2n_{\text{th}})\Gamma g^2 \frac{16\Delta + (\Gamma + \gamma)(\Gamma - 3\gamma)}{32\Delta^2(\Gamma + \gamma)}, \\ \eta_{21} &= \frac{g}{8\Delta} \left[ \frac{(\Gamma - \gamma)n_{\text{th}}}{2} + 2\sqrt{\Delta}(n_{\text{th}} + 1) - \frac{\Gamma(1 + 2n_{\text{th}})}{2} \frac{4\sqrt{\Delta} + (\Gamma - \gamma)}{4\sqrt{\Delta} + (\Gamma + \gamma)} \right], \\ \eta_{22} &= -\frac{g}{8\Delta} \left[ -\frac{(\Gamma - \gamma)n_{\text{th}}}{2} + 2\sqrt{\Delta}(n_{\text{th}} + 1) + \frac{\Gamma(1 + 2n_{\text{th}})}{2} \frac{4\sqrt{\Delta} - (\Gamma - \gamma)}{4\sqrt{\Delta} - (\Gamma + \gamma)} \right], \\ \eta_{23} &= \frac{g}{8\Delta} \left[ -(\Gamma - \gamma)n_{\text{th}} + \frac{(\Gamma^2 - \gamma^2)\Gamma(1 + 2n_{\text{th}})}{(\Gamma + \gamma)^2} \right], \\ \eta_{24} &= \frac{\gamma\Gamma g(1 + 2n_{\text{th}})}{4\Delta(\Gamma + \gamma)}, \\ \eta_{31} &= \frac{g^2}{8\Delta} \left[ 2(n_{\text{th}} + 1) - \frac{\Gamma - \gamma}{2g} - \frac{2(\gamma + \Gamma(2n_{\text{th}} + 1))}{4\sqrt{\Delta} + (\Gamma + \gamma)} \right], \\ \eta_{32} &= \frac{g^2}{8\Delta} \left[ 2(n_{\text{th}} + 1) + \frac{\Gamma - \gamma}{2g} + \frac{2(\gamma + \Gamma(2n_{\text{th}} + 1))}{4\sqrt{\Delta} + (\Gamma + \gamma)} \right], \\ \eta_{33} &= \frac{g^2(\Gamma - \gamma)(1 + n_{\text{th}})}{2\Delta(\Gamma + \gamma)}, \\ \eta_{34} &= -\frac{g^2 [\Gamma(2n_{\text{th}} + 1) - \gamma] [16\Delta + (\Gamma + \gamma)^2]}{32\Delta^2(\Gamma + \gamma)}, \end{aligned} \quad (\text{B13})$$

with

$$\begin{aligned} \alpha_1 &= -\frac{\gamma + \Gamma}{2} - 2\sqrt{\frac{A + \Delta}{2}}, \\ \alpha_4 &= -\frac{\gamma + \Gamma}{2} + 2\sqrt{\frac{A + \Delta}{2}}, \\ \Delta &= g^2 + \frac{(\Gamma - \gamma)^2}{16} - \frac{(\Delta_a + \Delta_b)^2}{4}, \\ A &= \sqrt{\Delta^2 + \frac{(\Gamma - \gamma)^2(\Delta_a + \Delta_b)^2}{16}}. \end{aligned} \quad (\text{B14})$$

Actually, if we consider the phase-matching condition ( $\Delta_a = \Delta_b = 0$ ), the analytical expression of  $\lambda_-$  after some simplifications can be reduced to

$$\begin{aligned} \lambda_- &\approx \frac{1}{2} \frac{X}{Y}, \\ X &= 1 + \frac{\Gamma(\Gamma n_{\text{th}} - g)}{2g} t + (g^2 - \Gamma^2 n_{\text{th}}) t^2 + \frac{g(2g + 3\Gamma)}{3} (\Gamma n_{\text{th}}) t^3 + \frac{g^2(g^2 - 4\Gamma^2 n_{\text{th}})}{3} t^4 + \frac{4g^4(6g + 5\Gamma)}{15(2g - \Gamma)} (\Gamma n_{\text{th}}) t^5 \\ &\quad + \frac{2g^4(g^2 - 24\Gamma^2 n_{\text{th}})}{45} t^6 + \frac{g^6}{3} (\Gamma n_{\text{th}}) t^7 + \frac{g^8}{315} t^8 + \frac{4g^8}{45} (\Gamma n_{\text{th}}) t^9 + \frac{g^{10}}{50} (\Gamma n_{\text{th}}) t^{11}, \\ Y &= 1 + \frac{3g(2g + \Gamma)}{2} t^2 + (2g + \Gamma) g^3 t^4 \left( \frac{4}{3} + \frac{11}{15} g^2 t^2 + \frac{1}{5} g^4 t^4 + \frac{1}{26} g^6 t^6 \right). \end{aligned} \quad (\text{B15})$$

We show the accurate simulations of  $E_N$  and the approximated results evaluated by Eqs. (B15) in Fig. 4. We can see that approximated results agree well with the accurate simulations when the effective optoacoustic coupling strength is strong enough.

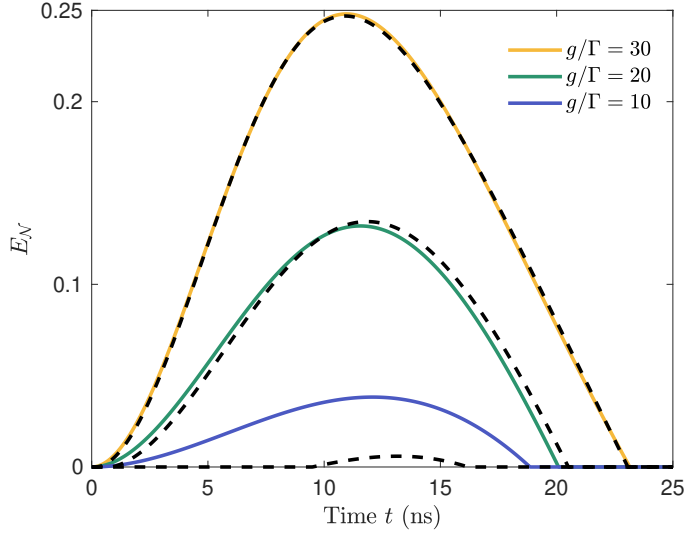


FIG. 4: (Color online) Time evolution of logarithmic negativity  $E_N$  at temperature of  $T_m = 30$  K for various ratios  $g/\Gamma$ , where solid curves denote the accurate simulation results of  $E_N$  and the black dashed curves correspond to the approximated solutions evaluated by Eqs. (B15).

Equations (B15) are cumbersome and complicated. Actually, we consider small evolution time to suppress the high thermal decoherence rate, i.e.,  $t \ll 1/\Gamma$ . Thus the characteristic behaviors of  $\lambda_-$  can be predicted by a simplified expression as follows

$$\lambda_- \approx \frac{1}{2} \times \frac{1 + g^2 t^2 + \frac{2}{3} g^2 (\Gamma n_{\text{th}}) t^3}{1 + 3g^2 t^2}, \quad (\text{B16})$$

where higher-order terms of  $t$  are ignored. If  $gt \ll 1$ , Eq. (B16) can be further reduced to

$$\lambda_- \approx \frac{1}{2} \left[ 1 - 2g^2 t^2 + \frac{2}{3} g^2 (\Gamma n_{\text{th}}) t^3 \right]. \quad (\text{B17})$$

### Appendix C: Entanglement at room temperature

In this section, we analyze the pulsed entanglement scheme for our system at room temperature (300 K). We consider the strong coupling regime and thus have the relation  $\mathcal{V}_{13}^2 \ll \mathcal{V}_{14}^2$  in our system when evolution time is small

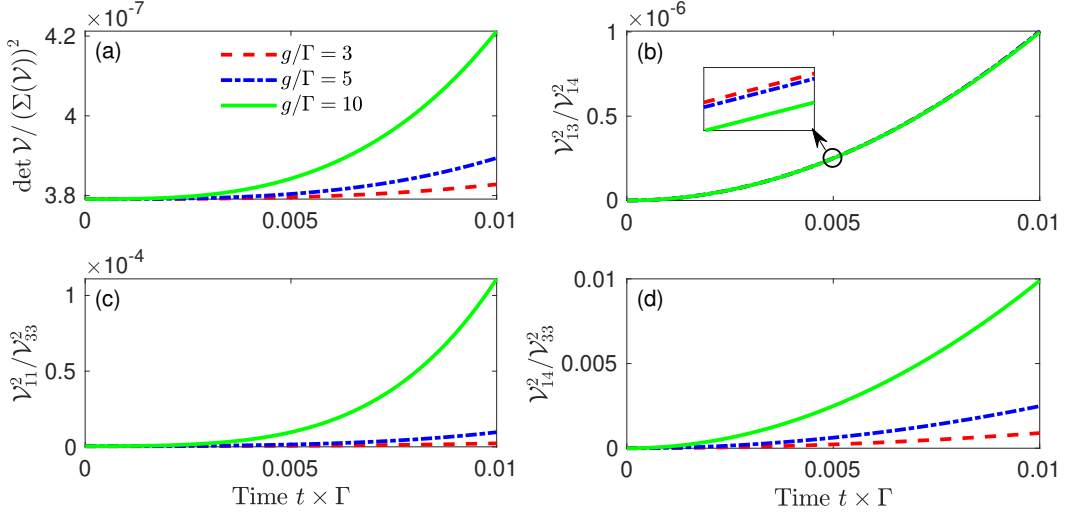


FIG. 5: (Color online) Time evolution of (a)  $\det \mathcal{V}/(\Sigma(\mathcal{V}))^2$  and (b)  $\mathcal{V}_{13}^2/\mathcal{V}_{14}^2$  for  $g/\Gamma = 3, 5, 10$ , where  $t \ll \Gamma^{-1}$ . Other parameters are  $\gamma/\Gamma = 0.02$ ,  $\Delta_a/\Gamma = 0.4$ ,  $\Delta_b/\Gamma = 4 \times 10^{-5}$ ,  $\Omega_{\text{ac}} = 7.7 \text{GHz}$  and room temperature  $T_m = 300 \text{K}$ .

( $t \ll \Gamma^{-1}$ ), as shown in Figs. 5 (a) and (b). Thus  $\lambda_-$  can be approximately calculated as

$$\begin{aligned}
 \lambda_- &= \sqrt{\frac{\Sigma(\mathcal{V}) - \sqrt{(\Sigma(\mathcal{V}))^2 - 4 \det \mathcal{V}}}{2}} \\
 &= \sqrt{\frac{\Sigma(\mathcal{V}) - \Sigma(\mathcal{V}) \sqrt{1 - \frac{4 \det \mathcal{V}}{(\Sigma(\mathcal{V}))^2}}}{2}} \\
 &\approx \sqrt{\frac{\det \mathcal{V}}{\Sigma(\mathcal{V})}} \\
 &\approx \frac{|\mathcal{V}_{13}^2 + \mathcal{V}_{14}^2 - \mathcal{V}_{11}\mathcal{V}_{33}|}{\sqrt{\mathcal{V}_{11}^2 + \mathcal{V}_{33}^2 + 2(\mathcal{V}_{13}^2 + \mathcal{V}_{14}^2)}} \\
 &\approx \frac{|\mathcal{V}_{14}^2 - \mathcal{V}_{11}\mathcal{V}_{33}|}{\sqrt{\mathcal{V}_{11}^2 + \mathcal{V}_{33}^2 + 2\mathcal{V}_{14}^2}}. \tag{C1}
 \end{aligned}$$

As  $\mathcal{V}_{11}^2 \ll \mathcal{V}_{33}^2$  and  $\mathcal{V}_{14}^2 \ll \mathcal{V}_{33}^2$  when  $t \ll \Gamma^{-1}$ , as shown in Figs. 5 (c) and (d),  $\lambda_-$  can be further reduced to

$$\begin{aligned}
 \lambda_- &\approx \frac{|\mathcal{V}_{14}^2 - \mathcal{V}_{11}\mathcal{V}_{33}|}{\mathcal{V}_{33}\sqrt{1 + 2\frac{\mathcal{V}_{14}^2}{\mathcal{V}_{33}^2}}} \\
 &\approx \frac{|\mathcal{V}_{14}^2 - \mathcal{V}_{11}\mathcal{V}_{33}|}{\mathcal{V}_{33} + \frac{\mathcal{V}_{14}^2}{\mathcal{V}_{33}}} \\
 &\approx \frac{|\mathcal{V}_{33}\mathcal{V}_{14}^2 - \mathcal{V}_{11}\mathcal{V}_{33}^2|}{\mathcal{V}_{33}^2 + \mathcal{V}_{14}^2}. \tag{C2}
 \end{aligned}$$

This means that the minimal symplectic eigenvalue  $\lambda_-$  is mainly dependent on three independent elements  $\mathcal{V}_{11}$ ,  $\mathcal{V}_{33}$ , and  $\mathcal{V}_{14}$ . In fact, these three elements of matrix  $\mathcal{V}$  can be approximately expressed as

$$\begin{aligned}
 \mathcal{V}_{11} &\approx \frac{1}{4} \left[ 2 + (\Gamma - \gamma)t + \frac{16g^2(n_{\text{th}} + 1)}{4}t^2 + \frac{16g^2(n_{\text{th}} + 1)}{12}\Delta t^4 \right] e^{-\frac{\gamma+\Gamma}{2}t} + \frac{\gamma g^2}{2\Delta}t + \frac{\Gamma g^2(2n_{\text{th}} + 1)}{6}t^3, \\
 \mathcal{V}_{33} &\approx \left( \frac{1}{2} - \frac{\Gamma - \gamma}{4}t + \frac{n_{\text{th}} + 1}{2n_{\text{th}} + 1}g^2t^2 \right) (2n_{\text{th}} + 1)e^{-\frac{\gamma+\Gamma}{2}t} + \frac{\Gamma(2n_{\text{th}} + 1)}{2}t - \frac{g^2\Gamma^2(2n_{\text{th}} + 1)}{4\Delta}t^2, \\
 \mathcal{V}_{14} &\approx \frac{gn_{\text{th}}}{4} \left[ -4(1 + \frac{1}{n_{\text{th}}}) + (\Gamma - \gamma)t - \frac{8}{3}\Delta t^2 \right] te^{-\frac{\gamma+\Gamma}{2}t} + \frac{g\Gamma}{4}(1 + 2n_{\text{th}}) \left( \frac{\Gamma^2}{16\Delta} - 1 \right) t^2, \tag{C3}
 \end{aligned}$$

where  $\Delta = g^2 + \frac{(\Gamma-\gamma)^2}{16} - \frac{(\Delta_a+\Delta_b)^2}{4}$ . We substitute Eq. (C3) into Eq. (C2) and use the first-order approximation, i.e.,  $\exp[-(\gamma + \Gamma)t/2] \approx 1 - (\gamma + \Gamma)t/2$ , when the evolution time is short, then  $\lambda_-$  can be approximately expressed as

$$\lambda_- \approx \frac{1}{2} \left| \frac{1 + (g^2 - \frac{\Gamma^2 - \gamma^2}{4})t^2 + \frac{g^2(3\Gamma^2 + 16g^2)}{24g^2}(\Gamma n_{\text{th}})t^3}{1 + 3g^2t^2} \right|, \quad (\text{C4})$$

If  $gt \ll 1$ , the above equation can be further simplified as follows

$$\lambda_- \approx \frac{1}{2} \left[ 1 - 2g^2t^2 + \frac{2}{3}g^2(\Gamma n_{\text{th}})t^3 \right]. \quad (\text{C5})$$

Given the parameters used in Fig. 5, we show the time evolution of  $E_N$  in the strong coupling regime in Fig. 6, where the solid curves denote accurate simulation results based on Eq. (B6) and Eq. (B8) and the dashed curves correspond to the approximated solutions based on Eq. (C4). Approximated results agree well with accurate analytical solutions. It shows that similar to the case at 30 K, there is a time window which allows optoacoustic entanglement generation between Stokes photons and acoustic phonons in our system.

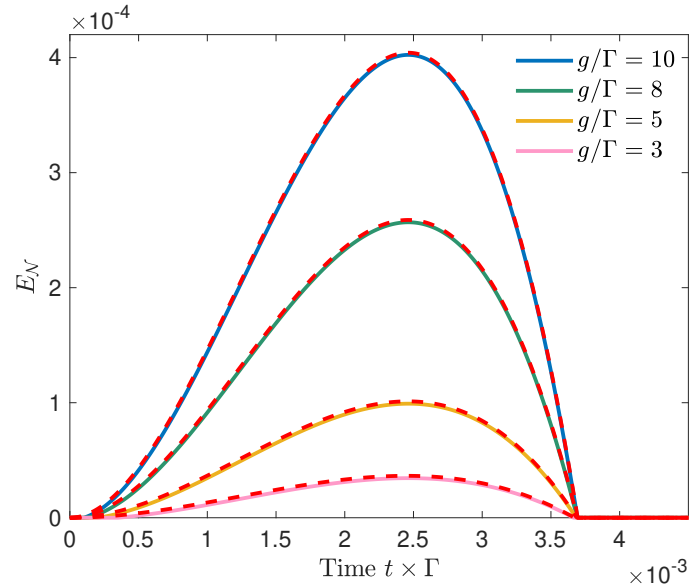


FIG. 6: (Color online) Time evolution of  $E_N$  for different coupling strength at room temperature  $T_m = 300$  K, where solid curves and red dashed curves correspond to the accurate simulation results and approximated solutions evaluated by Eq. (C4), respectively.

#### Appendix D: State transfer via Brillouin anti-Stokes scattering

In the main text, we use the Brillouin anti-Stokes interaction to achieve the state transfer between acoustic phonons and anti-Stokes photons. Now we present more details about this state transfer in this section. For a typical Brillouin-active waveguide, the dynamics of the backward Brillouin anti-Stokes scattering can be given by

$$\begin{aligned} \frac{\partial \tilde{a}_p}{\partial t} - v_{\text{opt}} \frac{\partial \tilde{a}_p}{\partial z} &= -\frac{\gamma}{2} \tilde{a}_p - ig_0^* \tilde{a}_{\text{as}} b_{\text{ac}}^\dagger + \sqrt{\gamma} \tilde{\xi}_p, \\ \frac{\partial \tilde{a}_{\text{as}}}{\partial t} + v_{\text{opt}} \frac{\partial \tilde{a}_{\text{as}}}{\partial z} &= -\frac{\gamma}{2} \tilde{a}_{\text{as}} - ig_0 \tilde{a}_p b_{\text{ac}} + \sqrt{\gamma} \tilde{\xi}_{\text{as}}, \\ \frac{\partial b_{\text{ac}}}{\partial t} + v_{\text{ac}} \frac{\partial b_{\text{ac}}}{\partial z} &= -\frac{\Gamma}{2} b_{\text{ac}} - ig_0 \tilde{a}_p^\dagger \tilde{a}_{\text{as}} + \sqrt{\Gamma} \tilde{\xi}_{\text{ac}}, \end{aligned} \quad (\text{D1})$$

where  $\tilde{a}_p$  is the envelope operator of the second pump laser and used to stimulate the anti-Stokes Brillouin interaction.  $b_{\text{ac}}$  denotes the envelope operator of the acoustic field generated during the entanglement generation process.  $\tilde{a}_{\text{as}}$

represents the envelope operator of the anti-Stokes field.  $\tilde{\xi}_p$  and  $\tilde{\xi}_{as}$  correspond to the Langevin noises. Here we choose the propagation direction of the acoustic field as the positive direction of axis  $z$ . Considering an undepleted pump, this three-field interaction can be reduced to an effective optoacoustic interaction between anti-Stokes photons and acoustic phonons and thus Eq. (D1) can be re-written as

$$\begin{aligned}\frac{\partial \tilde{a}_{as}}{\partial t} + v_{opt} \frac{\partial \tilde{a}_{as}}{\partial z} &= -\frac{\gamma}{2} \tilde{a}_{as} - i\tilde{g}b_{ac} + \sqrt{\gamma}\tilde{\xi}_{as}, \\ \frac{\partial b_{ac}}{\partial t} + v_{ac} \frac{\partial b_{ac}}{\partial z} &= -\frac{\Gamma}{2}b_{ac} - i\tilde{g}\tilde{a}_{as} + \sqrt{\Gamma}\xi_{ac},\end{aligned}\quad (D2)$$

where  $\tilde{g} = g_0 \sqrt{\langle \tilde{a}_p^\dagger \tilde{a}_p \rangle}$  is the pump-enhanced coupling strength which is tuned by the pump power. Actually, similar to the acoustic field  $b_{ac}$  in Eq. (A4), the anti-Stokes field  $\tilde{a}_{as}$  denotes the envelope operator with continuum modes and can be expressed in the discrete variable representation, i.e.,  $\tilde{a}_{as} = 1/\sqrt{2\pi} \int \tilde{a}(t, k) e^{ikz} dk$ , where  $\tilde{a}(t, k)$  corresponds to the annihilation operator for the  $k$ -th anti-Stokes photon mode with wavenumber  $k$ . Moving into the momentum space, the dynamics of this linearized anti-Stokes Brillouin interaction can be given by

$$\begin{aligned}\frac{db}{dt} &= -\left(\frac{\Gamma}{2} + i\Delta_b\right)b - i\tilde{g}\tilde{a} + \sqrt{\Gamma}\xi_b, \\ \frac{d\tilde{a}}{dt} &= -\left(\frac{\gamma}{2} + i\Delta_{\tilde{a}}\right)\tilde{a} - i\tilde{g}b + \sqrt{\gamma}\xi_{\tilde{a}},\end{aligned}\quad (D3)$$

where  $\Delta_{\tilde{a}} = kv_{opt}$  is the wavenumber-induced frequency shift for anti-Stokes photons and  $\xi_{\tilde{a}}$  is the Fourier transform of Langevin noise  $\tilde{\xi}_{as}$  and a zero-mean quantum Gaussian noise with  $\langle \xi_{\tilde{a}}(t_1) \xi_{\tilde{a}}^\dagger(t_2) \rangle = \delta(t_1 - t_2)$ . Eqs. (D3) are ordinary differential equations with constant coefficients, which can be analytically solved. Thus the analytical expression of the transferred anti-Stokes mode during time period  $t \in [\Delta\tau, \Delta\tau + \tau_2]$  can be given by

$$\begin{aligned}\tilde{a}(t) &= \left( \tilde{\mu}_2 e^{\tilde{\omega}_+(t-\Delta\tau)} - \tilde{\mu}_3 e^{\tilde{\omega}_-(t-\Delta\tau)} \right) \tilde{a}(\Delta\tau) + \tilde{\mu}_1 \left( e^{\tilde{\omega}_+(t-\Delta\tau)} - e^{\tilde{\omega}_-(t-\Delta\tau)} \right) b(\Delta\tau) \\ &\quad + \sqrt{\gamma} \int_{\Delta\tau}^t \left[ \tilde{\mu}_2 e^{\tilde{\omega}_+(t-\tau)} - \tilde{\mu}_3 e^{\tilde{\omega}_-(t-\tau)} \right] \xi_{\tilde{a}}(\tau) d\tau + \sqrt{\Gamma} \tilde{\mu}_1 \int_{\Delta\tau}^t \left[ e^{\tilde{\omega}_+(t-\tau)} - e^{\tilde{\omega}_-(t-\tau)} \right] \xi_b(\tau) d\tau,\end{aligned}\quad (D4)$$

with

$$\begin{aligned}\tilde{\omega}_+ &= -\frac{\gamma + \Gamma}{4} - i\frac{\Delta_b + \Delta_{\tilde{a}}}{2} - i\frac{\sqrt{16\tilde{g}^2 - ((\Gamma - \gamma) - 2i(\Delta_{\tilde{a}} - \Delta_b))^2}}{4}, \\ \tilde{\omega}_- &= -\frac{\gamma + \Gamma}{4} - i\frac{\Delta_b + \Delta_{\tilde{a}}}{2} + i\frac{\sqrt{16\tilde{g}^2 - ((\Gamma - \gamma) - 2i(\Delta_{\tilde{a}} - \Delta_b))^2}}{4}, \\ \tilde{\tau}_+ &= \frac{2(\Delta_{\tilde{a}} - \Delta_b) + i(\Gamma - \gamma)}{4\tilde{g}} + \frac{\sqrt{16\tilde{g}^2 - ((\Gamma - \gamma) - 2i(\Delta_{\tilde{a}} - \Delta_b))^2}}{4\tilde{g}}, \\ \tilde{\tau}_- &= \frac{2(\Delta_{\tilde{a}} - \Delta_b) + i(\Gamma - \gamma)}{4\tilde{g}} - \frac{\sqrt{16\tilde{g}^2 - ((\Gamma - \gamma) - 2i(\Delta_{\tilde{a}} - \Delta_b))^2}}{4\tilde{g}},\end{aligned}\quad (D5)$$

and

$$\tilde{\mu}_1 = \frac{1}{\tilde{\tau}_+ - \tilde{\tau}_-}, \quad \tilde{\mu}_2 = \frac{\tilde{\tau}_+}{\tilde{\tau}_+ - \tilde{\tau}_-}, \quad \tilde{\mu}_3 = \frac{\tilde{\tau}_-}{\tilde{\tau}_+ - \tilde{\tau}_-}, \quad (D6)$$

where  $\Delta\tau = \tau_1 + \tau_d$ . Here we assume that there is no anti-Stokes photon present at initial time, i.e.,  $N_{as}(\Delta\tau) = 0$ . Equation (D4) indicates that the generated anti-Stokes mode follows the dynamics of the acoustic mode, i.e., the state can be transferred from the existed acoustic phonons to the generated anti-Stokes photons. In order to investigate the influence of the thermal noise on such phonon-photon state transfer, we calculate the generated mean photon number for the anti-Stokes mode, which can be given by

$$N_{as}(t) = \langle \tilde{a}^\dagger(t) \tilde{a}(t) \rangle = |\tilde{\mu}_1|^2 \left| e^{\tilde{\omega}_+(t-\Delta\tau)} - e^{\tilde{\omega}_-(t-\Delta\tau)} \right|^2 N_b(\Delta\tau) + \Gamma |\tilde{\mu}_1|^2 n_{th} \int_{\Delta\tau}^t \left| e^{\tilde{\omega}_+(t-\tau)} - e^{\tilde{\omega}_-(t-\tau)} \right|^2 d\tau. \quad (D7)$$

The transferred anti-Stokes photon occupancy in the strong coupling regime can be simplified as follows

$$N_{as}(t) \approx \frac{1}{2} e^{-\frac{\gamma+\Gamma}{2}(t-\Delta\tau)} [1 - \cos(2\tilde{g}(t - \Delta\tau))] n_b, \quad (\text{D8})$$

where  $n_b = N_b(\Delta\tau)$  corresponds to the the initial phonon occupation for the readout process. Here we assume that the evolution time of the anti-Stokes process is short. The Rabi-oscillation property of  $N_{as}$  implies that the quantum states can be transferred between acoustic phonons and anti-Stokes photons via the anti-Stokes process.

For the entanglement readout process in the main text, we assume that the origin of time is taken at  $\tau_1 + \tau_d$ , i.e.,  $t \in [0, \tau_1 + \tau_d]$ , the transferred anti-Stokes photon occupation can be re-written as

$$N_{as}(t) \approx \frac{1}{2} e^{-\frac{\gamma+\Gamma}{2}t} [1 - \cos(2\tilde{g}t)] n_b, \quad (\text{D9})$$

where  $n_b$  denotes the initial Stokes photon occupation, i.e.,  $n_b = N_b(\tau_1 + \tau_d)$ .

### Appendix E: Entanglement measurement

As the quantum state of the acoustic phonons can be transferred to the anti-Stokes photons via the Brillouin anti-Stokes process, the entanglement between the Stokes photons and acoustic phonons can be demonstrated by quantifying the inseparability between the Stokes and anti-Stokes photons. In this subsection, we discuss how to calculate the logarithmic negativity  $\tilde{E}_{\mathcal{N}}$  between the optical Stokes field and transferred optical anti-Stokes field during the entanglement measurement period, i.e.,  $t \in [\tau_1 + \tau_d, \tau_1 + \tau_d + \tau_2]$ .

According to Eq. (A7), the Stoke and acoustic modes at time  $t = \tau_1$  can be given by

$$\begin{aligned} a(\tau_1) &= (\mu_2 e^{\omega_+ \tau_1} - \mu_3 e^{\omega_- \tau_1}) a(0) + (-e^{\omega_+ \tau_1} + e^{\omega_- \tau_1}) \mu_1 b^\dagger(0) + \sqrt{\gamma} \int_0^{\tau_1} [\mu_2 e^{\omega_+(\tau_1 - \tau)} - \mu_3 e^{\omega_-(\tau_1 - \tau)}] \xi_a(\tau) d\tau \\ &\quad + \sqrt{\Gamma} \mu_1 \int_0^{\tau_1} [-e^{\omega_+(\tau_1 - \tau)} + e^{\omega_-(\tau_1 - \tau)}] \xi_b^\dagger(\tau) d\tau, \\ b(\tau_1) &= \mu_1^* \left( e^{\omega_+^* \tau_1} - e^{\omega_-^* \tau_1} \right) a^\dagger(0) + \left( -\mu_3^* e^{\omega_+^* \tau_1} + \mu_2^* e^{\omega_-^* \tau_1} \right) b(0) + \sqrt{\gamma} \int_0^{\tau_1} [e^{\omega_+^*(\tau_1 - \tau)} - e^{\omega_-^*(\tau_1 - \tau)}] \xi_a^\dagger(\tau) d\tau \\ &\quad + \sqrt{\Gamma} \int_0^{\tau_1} [-\mu_3^* e^{\omega_+^*(\tau_1 - \tau)} + \mu_2^* e^{\omega_-^*(\tau_1 - \tau)}] \xi_b(\tau) d\tau. \end{aligned} \quad (\text{E1})$$

In addition, we assume that the output Stokes field produced during the entanglement generation process is fed into a single mode fiber and the corresponding dynamics can be given by

$$\frac{da}{dt} = - \left( \frac{\tilde{\gamma}}{2} + i\Delta_a \right) a_s + \sqrt{\tilde{\gamma}} \tilde{\xi}_a(t), \quad (\text{E2})$$

where  $\tilde{\gamma}$  is the optical loss rate of the Stokes field in the single mode fiber and  $\tilde{\xi}_a$  is the Langevin noise. The analytical solution of the above equation can be expressed as

$$a(t) = a(\tau_1) e^{-(\tilde{\gamma}/2 + i\Delta_a)(t - \tau_1)} + \sqrt{\tilde{\gamma}} \int_{\tau_1}^t e^{-(\tilde{\gamma}/2 + i\Delta_a)(t - \tau)} \tilde{\xi}_a(\tau) d\tau. \quad (\text{E3})$$

Furthermore, the acoustic field in the sample during the delay time period, i.e.,  $t \in [\tau_1, \tau_1 + \tau_d]$ , is driven by the thermal noise and its dynamics can be given by

$$\frac{db}{dt} = - \left( \frac{\Gamma}{2} + i\Delta_b \right) b + \sqrt{\Gamma} \xi_b. \quad (\text{E4})$$

The analytical solution of  $b$  can be expressed as

$$b(t) = b(\tau_1) e^{-(\Gamma/2 + i\Delta_b)(t - \tau_1)} + \sqrt{\Gamma} \int_{\tau_1}^t e^{-(\Gamma/2 + i\Delta_b)(t - \tau)} \xi_b(\tau) d\tau. \quad (\text{E5})$$

Therefore, the initial states for the entanglement measurement process, i.e., at time  $t = \tau_1 + \tau_d$ , can be expressed as

$$\begin{aligned}
a(\tau_1 + \tau_d) &= (\mu_2 e^{\omega_+ \tau_1} - \mu_3 e^{\omega_- \tau_1}) e^{-(\tilde{\gamma}/2 + i\Delta_a) \tau_d} a_s(0) + (-e^{\omega_+ \tau_1} + e^{\omega_- \tau_1}) \mu_1 e^{-(\tilde{\gamma}/2 + i\Delta_a) \tau_d} b^\dagger(0) \\
&\quad + \sqrt{\gamma} e^{-(\tilde{\gamma}/2 + i\Delta_a) \tau_d} \int_0^{\tau_1} \left( \mu_2 e^{\omega_+(\tau_1 - \tau)} - \mu_3 e^{\omega_-(\tau_1 - \tau)} \right) \xi_a(\tau) d\tau \\
&\quad + \sqrt{\Gamma} \mu_1 e^{-(\tilde{\gamma}/2 + i\Delta_a) \tau_d} \int_0^{\tau_1} \left( -e^{\omega_+(\tau_1 - \tau)} + e^{\omega_-(\tau_1 - \tau)} \right) \xi_b^\dagger(\tau) d\tau \\
&\quad + \sqrt{\tilde{\gamma}} e^{-(\tilde{\gamma}/2 + i\Delta_a) (\tau_1 + \tau_d)} \int_{\tau_1}^{\tau_1 + \tau_d} e^{(\tilde{\gamma}/2 + i\Delta_a) \tau} \tilde{\xi}_a(\tau) d\tau, \\
b(\tau_1 + \tau_d) &= \mu_1^* \left( e^{\omega_+^* \tau_1} - e^{\omega_-^* \tau_1} \right) e^{-(\Gamma/2 + i\Delta_b) \tau_d} a^\dagger(0) + \left( -\mu_3^* e^{\omega_+^* \tau_1} + \mu_2^* e^{\omega_-^* \tau_1} \right) e^{-(\Gamma/2 + i\Delta_b) \tau_d} b(0) \\
&\quad + \sqrt{\gamma} \mu_1^* e^{-(\Gamma/2 + i\Delta_b) \tau_d} \int_0^{\tau_1} \left( e^{\omega_+^*(\tau_1 - \tau)} - e^{\omega_-^*(\tau_1 - \tau)} \right) \xi_a^\dagger(\tau) d\tau \\
&\quad + \sqrt{\Gamma} e^{-(\Gamma/2 + i\Delta_b) \tau_d} \int_0^{\tau_1} \left( -\mu_3^* e^{\omega_+^*(\tau_1 - \tau)} + \mu_2^* e^{\omega_-^*(\tau_1 - \tau)} \right) \xi_b(\tau) d\tau \\
&\quad + \sqrt{\Gamma} e^{-(\Gamma/2 + i\Delta_b) (\tau_1 + \tau_d)} \int_{\tau_1}^{\tau_1 + \tau_d} e^{(\Gamma/2 + i\Delta_b) \tau} \xi_b(\tau) d\tau. \tag{E6}
\end{aligned}$$

The state of the anti-Stokes mode  $\tilde{a}$  at time  $t = \tau_1 + \tau_d$  is the vacuum state. Thus the optical Stokes mode  $a(t)$  and anti-Stokes mode  $\tilde{a}(t)$  during time  $t \in [\Delta\tau, \Delta\tau + \tau_2]$  can be given by

$$\begin{aligned}
a(t) &= a(\Delta\tau) e^{-(\tilde{\gamma}/2 + i\Delta_a)(t - \Delta\tau)} + \sqrt{\tilde{\gamma}} \int_{\Delta\tau}^t e^{-(\tilde{\gamma}/2 + i\Delta_a)(t - \tau)} \tilde{\xi}_a(\tau) d\tau, \\
\tilde{a}(t) &= \left( \tilde{\mu}_2 e^{\tilde{\omega}_+(t - \Delta\tau)} - \tilde{\mu}_3 e^{\tilde{\omega}_-(t - \Delta\tau)} \right) a(\Delta\tau) + \tilde{\mu}_1 \left( e^{\tilde{\omega}_+(t - \Delta\tau)} - e^{\tilde{\omega}_-(t - \Delta\tau)} \right) b(\Delta\tau) \\
&\quad + \sqrt{\gamma} \int_{\Delta\tau}^t \left( \tilde{\mu}_2 e^{\tilde{\omega}_+(\tau - \Delta\tau)} - \tilde{\mu}_3 e^{\tilde{\omega}_-(\tau - \Delta\tau)} \right) \xi_{\tilde{a}}(\tau) d\tau + \sqrt{\Gamma} \tilde{\mu}_1 \int_{\Delta\tau}^t \left( e^{\tilde{\omega}_+(\tau - \Delta\tau)} - e^{\tilde{\omega}_-(\tau - \Delta\tau)} \right) \xi_b(\tau) d\tau. \tag{E7}
\end{aligned}$$

Now we utilize the logarithmic negativity  $\tilde{E}_{\mathcal{N}}$  to quantify the inseparability between the Stokes mode  $a$  and anti-Stokes mode  $\tilde{a}$  during the entanglement measurement process. We define the quadrature operators as follows

$$\begin{aligned}
x_1 &= \frac{a + a^\dagger}{\sqrt{2}}, \quad p_1 = \frac{a - a^\dagger}{i\sqrt{2}}, \\
x_3 &= \frac{\tilde{a} + \tilde{a}^\dagger}{\sqrt{2}}, \quad p_3 = \frac{\tilde{a} - \tilde{a}^\dagger}{i\sqrt{2}}. \tag{E8}
\end{aligned}$$

The corresponding covariance matrix  $\tilde{\mathcal{V}}$  can be given by

$$\tilde{\mathcal{V}}_{i,j} = \frac{\langle \phi_i(t) \phi_j(t) + \phi_i(t) \phi_j(t) \rangle}{2} - \langle \phi_i(t) \rangle \langle \phi_j(t) \rangle, \tag{E9}$$

where  $\phi^T(t) = (x_1(t), p_1(t), x_3(t), p_3(t))$ . Substituting Eqs. (E7) into Eq. (E9), the symmetrical covariance matrix  $\tilde{E}_{\mathcal{N}}$  can be given by

$$\tilde{\mathcal{V}} = \begin{bmatrix} \tilde{\mathcal{V}}_{11} & 0 & \tilde{\mathcal{V}}_{13} & \tilde{\mathcal{V}}_{14} \\ 0 & \tilde{\mathcal{V}}_{11} & \tilde{\mathcal{V}}_{14} & -\tilde{\mathcal{V}}_{13} \\ \tilde{\mathcal{V}}_{13} & \tilde{\mathcal{V}}_{14} & \tilde{\mathcal{V}}_{33} & 0 \\ \tilde{\mathcal{V}}_{14} & -\tilde{\mathcal{V}}_{13} & 0 & \tilde{\mathcal{V}}_{33} \end{bmatrix}, \tag{E10}$$

where

$$\begin{aligned}
\tilde{\mathcal{V}}_{11} &= \frac{1 - e^{-\tilde{\gamma}(t-\Delta\tau)}}{2} + \frac{e^{-\tilde{\gamma}(t-\Delta\tau)}}{2} (\langle a(\Delta\tau)^\dagger a(\Delta\tau) \rangle + \langle a(\Delta\tau) a^\dagger(\Delta\tau) \rangle), \\
\tilde{\mathcal{V}}_{13} &= e^{-(\tilde{\gamma}/2+i\Delta_a)(t-\Delta\tau)} \left( e^{\tilde{\omega}_+(t-\Delta\tau)} - e^{\tilde{\omega}_-(t-\Delta\tau)} \right) \tilde{\mu}_1 \frac{\langle a(\Delta\tau) b(\Delta\tau) \rangle + \langle b(\Delta\tau) a(\Delta\tau) \rangle}{4} \\
&\quad + e^{-(\tilde{\gamma}/2-i\Delta_a)(t-\Delta\tau)} \left( e^{\tilde{\omega}_+^*(t-\Delta\tau)} - e^{\tilde{\omega}_-^*(t-\Delta\tau)} \right) \tilde{\mu}_1^* \frac{\langle a^\dagger(\Delta\tau) b^\dagger(\Delta\tau) \rangle + \langle b^\dagger(\Delta\tau) a^\dagger(\Delta\tau) \rangle}{4}, \\
\tilde{\mathcal{V}}_{14} &= -ie^{-(\tilde{\gamma}/2+i\Delta_a)(t-\Delta\tau)} \left( e^{\tilde{\omega}_+(t-\Delta\tau)} - e^{\tilde{\omega}_-(t-\Delta\tau)} \right) \tilde{\mu}_1 \frac{\langle a(\Delta\tau) b(\Delta\tau) \rangle + \langle b(\Delta\tau) a(\Delta\tau) \rangle}{4} \\
&\quad + ie^{-(\tilde{\gamma}/2-i\Delta_a)(t-\Delta\tau)} \left( e^{\tilde{\omega}_+^*(t-\Delta\tau)} - e^{\tilde{\omega}_-^*(t-\Delta\tau)} \right) \tilde{\mu}_1^* \frac{\langle a^\dagger(\Delta\tau) b^\dagger(\Delta\tau) \rangle + \langle b^\dagger(\Delta\tau) a^\dagger(\Delta\tau) \rangle}{4}, \\
\tilde{\mathcal{V}}_{33} &= \frac{|\tilde{\mu}_2 e^{\tilde{\omega}_+(t-\Delta\tau)} - \tilde{\mu}_3 e^{\tilde{\omega}_-(t-\Delta\tau)}|^2}{2} \\
&\quad + \frac{\gamma}{2} \left[ \frac{|\tilde{\mu}_2|^2}{\tilde{\alpha}_1} \left( e^{\tilde{\alpha}_1(t-\Delta\tau)} - 1 \right) - \frac{\tilde{\mu}_2 \tilde{\mu}_3^*}{\tilde{\alpha}_2} \left( e^{\tilde{\alpha}_2(t-\Delta\tau)} - 1 \right) - \frac{\tilde{\mu}_3 \tilde{\mu}_2^*}{\tilde{\alpha}_3} \left( e^{\tilde{\alpha}_3(t-\Delta\tau)} - 1 \right) + \frac{|\tilde{\mu}_3|^2}{\tilde{\alpha}_4} \left( e^{\tilde{\alpha}_4(t-\Delta\tau)} - 1 \right) \right] \\
&\quad + |\tilde{\mu}_1|^2 \left| e^{\tilde{\omega}_+(t-\Delta\tau)} - e^{\tilde{\omega}_-(t-\Delta\tau)} \right|^2 \frac{\langle b^\dagger(\Delta\tau) b(\Delta\tau) \rangle + \langle b(\Delta\tau) b^\dagger(\Delta\tau) \rangle}{2} \\
&\quad + \frac{\Gamma(1+2n_{\text{th}})}{2} |\tilde{\mu}_1|^2 \left[ \frac{e^{\tilde{\alpha}_1(t-\Delta\tau)} - 1}{\tilde{\alpha}_1} - \frac{e^{\tilde{\alpha}_2(t-\Delta\tau)} - 1}{\tilde{\alpha}_2} - \frac{e^{\tilde{\alpha}_3(t-\Delta\tau)} - 1}{\tilde{\alpha}_3} + \frac{e^{\tilde{\alpha}_4(t-\Delta\tau)} - 1}{\tilde{\alpha}_4} \right]. \tag{E11}
\end{aligned}$$

The coefficients  $\tilde{\alpha}_i$  can be given by

$$\begin{aligned}
\tilde{\alpha}_1 &= \tilde{\omega}_+ + \tilde{\omega}_+^*, \quad \tilde{\alpha}_2 = \tilde{\omega}_+ + \tilde{\omega}_-^*, \\
\tilde{\alpha}_3 &= \tilde{\omega}_- + \tilde{\omega}_-^*, \quad \tilde{\alpha}_4 = \tilde{\omega}_- + \tilde{\omega}_-^*. \tag{E12}
\end{aligned}$$

These correlation functions at time  $\Delta\tau$  can be calculated as follows

$$\begin{aligned}
\langle a^\dagger(\Delta\tau) a(\Delta\tau) \rangle &= (1+n_{\text{th}}) |\mu_1|^2 | -e^{\omega_+ \tau_1} + e^{\omega_- \tau_1} |^2 e^{-\tilde{\gamma} \tau_d} \\
&\quad + (1+n_{\text{th}}) \Gamma |\mu_1|^2 e^{-\tilde{\gamma} \tau_d} \left[ \frac{e^{\alpha_1 \tau_1} - 1}{\alpha_1} - \frac{e^{\alpha_2 \tau_1} - 1}{\alpha_2} - \frac{e^{\alpha_3 \tau_1} - 1}{\alpha_3} + \frac{e^{\alpha_4 \tau_1} - 1}{\alpha_4} \right], \\
\langle b(\Delta\tau) b^\dagger(\Delta\tau) \rangle &= (1+n_{\text{th}}) e^{-\Gamma \tau_d} | -\mu_3 e^{\omega_+ \tau_1} + \mu_2 e^{\omega_- \tau_1} |^2 + (1+n_{\text{th}}) (1 - e^{-\Gamma \tau_d}) \\
&\quad + \Gamma (1+n_{\text{th}}) e^{-\Gamma \tau_d} \left[ \frac{|\mu_3|^2}{\alpha_1} (e^{\alpha_1 \tau_1} - 1) - \frac{\mu_3 \mu_2^*}{\alpha_2} (e^{\alpha_2 \tau_1} - 1) - \frac{\mu_2 \mu_3^*}{\alpha_2} (e^{\alpha_3 \tau_1} - 1) + \frac{|\mu_2|^2}{\alpha_1} (e^{\alpha_4 \tau_1} - 1) \right], \\
\langle a(\Delta\tau) b(\Delta\tau) \rangle &= (\mu_2 e^{\omega_+ \tau_1} - \mu_3 e^{\omega_- \tau_1}) \mu_1^* \left( e^{\omega_+^* \tau_1} - e^{\omega_-^* \tau_1} \right) e^{-(\tilde{\gamma}/2+i\Delta_a) \tau_d} e^{-(\Gamma/2+i\Delta_b) \tau_d} \\
&\quad + n_{\text{th}} \left( -\mu_3^* e^{\omega_+^* \tau_1} + \mu_2^* e^{\omega_-^* \tau_1} \right) \mu_1 (e^{\omega_+ \tau_1} - e^{\omega_- \tau_1}) e^{-(\tilde{\gamma}/2+i\Delta_a) \tau_d} e^{-(\Gamma/2+i\Delta_b) \tau_d} \\
&\quad + \gamma \mu_1^* e^{-(\tilde{\gamma}/2+i\Delta_a) \tau_d} e^{-(\Gamma/2+i\Delta_b) \tau_d} \\
&\quad \times \left[ \frac{\mu_2 (e^{\alpha_1 \tau_1} - 1)}{\alpha_1} - \frac{\mu_2 (e^{\alpha_2 \tau_1} - 1)}{\alpha_2} - \frac{\mu_3 (e^{\alpha_3 \tau_1} - 1)}{\alpha_3} + \frac{\mu_3 (e^{\alpha_4 \tau_1} - 1)}{\alpha_4} \right] \\
&\quad + \Gamma n_{\text{th}} \mu_1 e^{-(\tilde{\gamma}/2+i\Delta_a) \tau_d} e^{-(\Gamma/2+i\Delta_b) \tau_d} \\
&\quad \times \left[ \frac{\mu_3^* (e^{\alpha_1 \tau_1} - 1)}{\alpha_1} - \frac{\mu_2^* (e^{\alpha_2 \tau_1} - 1)}{\alpha_2} - \frac{\mu_3^* (e^{\alpha_3 \tau_1} - 1)}{\alpha_3} + \frac{\mu_2^* (e^{\alpha_4 \tau_1} - 1)}{\alpha_4} \right], \\
\langle a^\dagger(\Delta\tau) b^\dagger(\Delta\tau) \rangle &= (1+n_{\text{th}}) \left( -e^{\omega_+^* \tau_1} + e^{\omega_-^* \tau_1} \right) \mu_1^* (-\mu_3 e^{\omega_+ \tau_1} + \mu_2 e^{\omega_- \tau_1}) e^{-(\tilde{\gamma}/2-i\Delta_a) \tau_d} e^{-(\Gamma/2-i\Delta_b) \tau_d} \\
&\quad + \Gamma (1+n_{\text{th}}) \mu_1^* e^{-(\tilde{\gamma}/2-i\Delta_a) \tau_d} e^{-(\Gamma/2-i\Delta_b) \tau_d} \\
&\quad \times \left[ \frac{\mu_3 (e^{\alpha_1 \tau_1} - 1)}{\alpha_1} - \frac{\mu_3 (e^{\alpha_2 \tau_1} - 1)}{\alpha_2} - \frac{\mu_2 (e^{\alpha_3 \tau_1} - 1)}{\alpha_3} + \frac{\mu_2 (e^{\alpha_4 \tau_1} - 1)}{\alpha_4} \right]. \tag{E13}
\end{aligned}$$

Therefore, the logarithmic negativity  $\tilde{E}_{\mathcal{N}}$  can be calculated as follows

$$\tilde{E}_{\mathcal{N}} = \max \left[ 0, \ln 2 \tilde{\lambda}_- \right], \tag{E14}$$

where

$$\tilde{\lambda}_- = \sqrt{\frac{\Sigma(\tilde{\mathcal{V}}) - \sqrt{(\Sigma(\tilde{\mathcal{V}}))^2 - 4 \det \tilde{\mathcal{V}}}}{2}}, \quad (\text{E15})$$

and

$$\begin{aligned} \Sigma(\tilde{\mathcal{V}}) &= \tilde{\mathcal{V}}_{11}^2 + \tilde{\mathcal{V}}_{33}^2 + 2 \left( \tilde{\mathcal{V}}_{13}^2 + \tilde{\mathcal{V}}_{14}^2 \right), \\ \det \tilde{\mathcal{V}} &= \left( \tilde{\mathcal{V}}_{13}^2 + \tilde{\mathcal{V}}_{14}^2 - \tilde{\mathcal{V}}_{11} \tilde{\mathcal{V}}_{33} \right)^2. \end{aligned} \quad (\text{E16})$$

As we consider the system parameters in the regime that  $g \gg \Gamma \gg \gamma$ ,  $\Gamma \gg \Delta_a = \Delta_{\tilde{a}} \gg \Delta_b$ ,  $\tau_d \gg \tau_{1,2}$ , and environmental temperature is tens of Kelvin, after some simplifications we have

$$\tilde{\lambda}_- \approx \left| \frac{(\tilde{\mathcal{V}}_{11} \tilde{\mathcal{V}}_{ss} - \tilde{\mathcal{V}}_{33}^2) (\tilde{\mathcal{V}}_{11} + \tilde{\mathcal{V}}_{33})}{\tilde{\mathcal{V}}_{11}^2 + \tilde{\mathcal{V}}_{33}^2 + \tilde{\mathcal{V}}_{11} \tilde{\mathcal{V}}_{33} + \tilde{\mathcal{V}}_{13}^2} \right|, \quad (\text{E17})$$

where

$$\begin{aligned} \tilde{\mathcal{V}}_{11} &\approx \frac{1 + 2n_s}{2}, \\ \tilde{\mathcal{V}}_{33} &\approx \frac{1 + 2n_{\text{th}}}{2} + \left[ \frac{n_b - 2n_{\text{th}}}{2} - \frac{n_b}{2} \cos(2\tilde{g}(t - \Delta\tau)) - \frac{\Gamma(1 + 2n_{\text{th}})}{8\tilde{g}} \sin(2\tilde{g}(t - \Delta\tau)) \right] e^{-\frac{\Gamma}{2}(t - \Delta\tau)}, \\ \tilde{\mathcal{V}}_{13} &\approx \frac{\mathcal{C}_{ns}}{2} \sin(\tilde{g}(t - \Delta\tau)) e^{-\frac{\Gamma}{4}(t - \Delta\tau)}, \end{aligned} \quad (\text{E18})$$

and

$$\begin{aligned} n_s &= \langle a^\dagger(\Delta\tau) a(\Delta\tau) \rangle, \\ n_b &= \langle b^\dagger(\Delta\tau) b(\Delta\tau) \rangle, \\ \mathcal{C}_{ns} &= \text{Im} [\langle a(\Delta\tau) b(\Delta\tau) \rangle + \langle b(\Delta\tau) a(\Delta\tau) \rangle]. \end{aligned} \quad (\text{E19})$$

Actually,  $n_s$  and  $n_b$  denote the Stokes photon occupation and acoustic phonon occupation at time  $\tau_1 + \tau_d$ .  $\mathcal{C}_{ns}$  corresponds to the cross-correlation between Stokes photons and acoustic phonons at time  $\tau_1 + \tau_d$ . Substituting Eqs. (E18) into Eq. (E17),  $\tilde{\lambda}_-$  can be simplified as follows

$$\tilde{\lambda}_- \approx \frac{1}{2} \left| \frac{\sum_{n=0}^{12} \eta_{1n} (t - \Delta\tau)^n}{\sum_{n=0}^{14} \eta_{2n} (t - \Delta\tau)^n} \right|, \quad (\text{E20})$$

with

$$\begin{aligned}
\eta_{10} &= \frac{1 + 3n_s + 2n_s^2}{4}, \\
\eta_{11} &= -\frac{\Gamma}{16}(3 + 8n_s + 4n_s^2), \\
\eta_{12} &= \tilde{g}^2 \frac{n_b(3 + 8n_s + 4n_s^2) - (1 + n_s)\mathcal{C}_{ns}^2}{4}, \\
\eta_{13} &= \Gamma \tilde{g}^2 \frac{(3 + 2n_s)(2 + 4n_s + 3\mathcal{C}_{ns}^2) + 4n_{th}(3 + 8n_s + 4n_s^2) - 6n_b(5 + 12n_s + 4n_s^2)}{48}, \\
\eta_{14} &= \tilde{g}^4 \frac{6n_b^2(1 + 2n_s) - n_b(3 + 8n_s + 4n_s^2) + (1 + n_s - 3n_b)\mathcal{C}_{ns}^2}{12}, \\
\eta_{15} &= -\Gamma \tilde{g}^4(1 + 2n_s) \frac{3 + 2n_s + 5n_b(12n_b - 2n_s - 9) + n_{th}(6 - 40n_b + 4n_s)}{120} \\
&\quad - \Gamma \tilde{g}^4 \frac{5 + 4n_{th} - 12n_b + 2n_s}{48} \mathcal{C}_{ns}^2, \\
\eta_{16} &= \tilde{g}^6 \frac{n_b(3 + 8n_s + 4n_s^2) - 30n_b^2(1 + 2n_s) - (1 + n_s - 15n_b)\mathcal{C}_{ns}^2}{90}, \\
\eta_{17} &= \Gamma \tilde{g}^2(1 + 2n_s) \frac{3 + 420n_b^2 + 2n_s - 7n_b(21 + 2n_s) + 2n_{th}(3 - 112n_b + 2n_s)}{1260} \\
&\quad + \Gamma \tilde{g}^6 \frac{11 + 16n_{th} - 60n_b + 2n_s}{360} \mathcal{C}_{ns}^2, \\
\eta_{18} &= \tilde{g}^8 \frac{126n_b^2(1 + 2n_s) - n_b(3 + 8n_s + 4n_s^2) + (1 + n_s - 63n_b)\mathcal{C}_{ns}^2}{120}, \\
\eta_{19} &= -\Gamma \tilde{g}^8(1 + 2n_s) \frac{3 + 2n_s + 3n_b(756n_b - 6n_s - 179) + 2n_{th}(3 - 492n_b + 2n_s)}{22680} \\
&\quad - \Gamma \tilde{g}^8 \frac{91 + 164n_{th} - 756n_b + 6n_s}{15120} \mathcal{C}_{ns}^2, \\
\eta_{110} &= \tilde{g}^{10} \frac{n_b(3 + 8n_s + 4n_s^2) - 510n_b^2(1 + 2n_s) - (1 + n_s - 256n_b)\mathcal{C}_{ns}^2}{28350}, \\
\eta_{111} &= \Gamma \tilde{g}^{10} \frac{n_b(1 + 2n_s)(-3 + 4n_{th} + 1020n_b - 2n_s) + (1 - n_{th} - 510n_b + n_s)S^2}{56700}, \\
\eta_{112} &= \tilde{g}^{12} \frac{n_b(1 + 2n_s)(2n_{th} + 1023n_b)}{467775} - \tilde{g}^{12} \frac{(n_{th} + 1023n_b)\mathcal{C}_{ns}^2}{935550}, \tag{E21}
\end{aligned}$$

and

$$\begin{aligned}
\eta_{20} &= \frac{1 + 3n_s + 2n_s^2}{2}, \\
\eta_{21} &= -\frac{\Gamma(3 + 2n_s)}{8}, \\
\eta_{22} &= \tilde{g}^2 \frac{2n_b(3 + 2n_s) + \mathcal{C}_{ns}^2}{4}, \\
\eta_{23} &= \Gamma \tilde{g}^2 \frac{6 + 4n_s + 4n_{th}(3 + 2n_s) - 6n_b(5 + 2n_s) - 3\mathcal{C}_{ns}^2}{24}, \\
\eta_{24} &= \tilde{g}^4 \frac{12n_b^2 - 2n_b(3 + 2n_s) - \mathcal{C}_{ns}^2}{12}, \\
\eta_{25} &= \Gamma \tilde{g}^4 \frac{-3 - 2n_s - 5n_b(12n_b - 9 - 2n_s) + n_{th}(-6 + 40n_b - 4n_s)}{60}, \\
\eta_{26} &= \tilde{g}^6 \frac{-60n_b^2 + 2n_b(3 + 2n_s) + \mathcal{C}_{ns}^2}{90}, \\
\eta_{27} &= \Gamma \tilde{g}^6 \frac{6 + 4n_s + 14n_b(60n_b - 21 - 2n_s) + 4n_{th}(3 - 112n_b + 2n_s) - 7\mathcal{C}_{ns}^2}{1260},
\end{aligned}$$

$$\begin{aligned}
\eta_{28} &= \tilde{g}^8 \frac{252n_b - 2n_b(3 + 2n_s) - \mathcal{C}_{ns}^2}{1260}, \\
\eta_{29} &= \Gamma \tilde{g}^8 \frac{-6 - 4n_s - 6n_b(756n_b - 6n_s - 179) + 4n_{th}(-3 + 492n_b - 2n_s) + 9\mathcal{C}_{ns}^2}{22680}, \\
\eta_{210} &= \tilde{g}^{10} \frac{2n_b(3 + 2n_s) - 1020n_b^2 + \mathcal{C}_{ns}^2}{28350}, \\
\eta_{211} &= -\Gamma \tilde{g}^{10} \frac{2n_b(3 - 4n_{th} + 2n_s) - 2040n_b^2 + \mathcal{C}_{ns}^2}{56700}, \\
\eta_{212} &= \tilde{g}^{12} \frac{n_b(2n_{th} + 1023n_b)}{233888}, \\
\eta_{213} &= -\Gamma \tilde{g}^{12} \frac{n_b(2n_{th} + 1023n_b)}{233888}, \\
\eta_{214} &= -\tilde{g}^{14} \frac{n_b^2}{2598}.
\end{aligned} \tag{E22}$$

We present the time evolution of  $\tilde{E}_{\mathcal{N}}$  in Fig. 7, where the solid curves denote the accurate solutions of  $\tilde{E}_{\mathcal{N}}$  versus different coupling strength  $\tilde{g}$  and red dashed curves correspond to the approximated solutions evaluated by Eq. (E20). Here, we assume that the coupling strength during the entanglement generation is  $g/\Gamma = 30$ , temperature is  $T_m = 30$  K, and delayed time is  $\tau_d = 0.1$  ns.

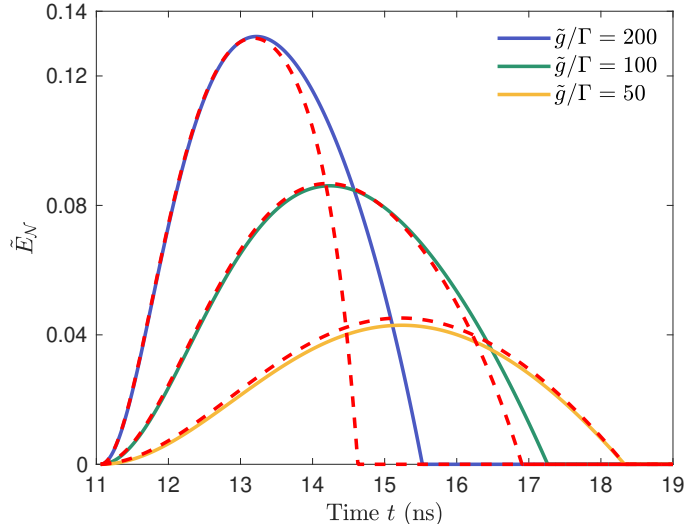


FIG. 7: (Color online) Time evolution of  $\tilde{E}_{\mathcal{N}}$  for different coupling strength at temperature 30 K, where solid curves and dashed curves denote the accurate simulation and corresponding approximated results, respectively.

However, the approximated expression of Eq. (E20) is still complicated. If we consider the small time  $\tilde{g}(t - \Delta\tau) \ll 1$ , Eq. (E20) can be further simplified by ignoring higher-order terms as follows

$$\tilde{\lambda}_- \approx \frac{1}{2} \left| \frac{1 + \tilde{\eta}_1(t - \Delta\tau)^2 + \tilde{\eta}_2^2(t - \Delta\tau)^3}{1 + \tilde{\eta}_3(t - \Delta\tau)^2} \right|, \tag{E23}$$

with

$$\begin{aligned}
\tilde{\eta}_1 &= \tilde{g}^2 \left[ \frac{n_b}{1 + n_s} + \frac{2n_b(1 + 2n_s) - \mathcal{C}_{ns}^2}{1 + 2n_s} \right], \\
\tilde{\eta}_2 &= \frac{2\tilde{g}^2(\Gamma n_{th})}{3}, \\
\tilde{\eta}_3 &= \tilde{g}^2 \left[ \frac{n_b}{1 + n_s} + \frac{4n_b + \mathcal{C}_{ns}^2}{2(1 + n_s)(1 + 2n_s)} \right].
\end{aligned} \tag{E24}$$

If  $\sqrt{\eta_3}(t - \Delta\tau) \ll 1$ , Eq. (E23) can be further reduced to

$$\tilde{\lambda}_- \approx \frac{1}{2} \left[ 1 - \eta^2(t - \Delta\tau)^2 + \frac{2}{3} \tilde{g}^2(\Gamma n_{\text{th}})(t - \Delta\tau)^3 \right], \quad (\text{E25})$$

where

$$\eta^2 = \frac{\tilde{g}^2(\mathcal{C}_{ns}^2 - 4n_b n_s)}{1 + 2n_s}. \quad (\text{E26})$$

We present the accurate simulation results and approximated analytical results evaluated by Eq. (E25) in Fig. 8. In

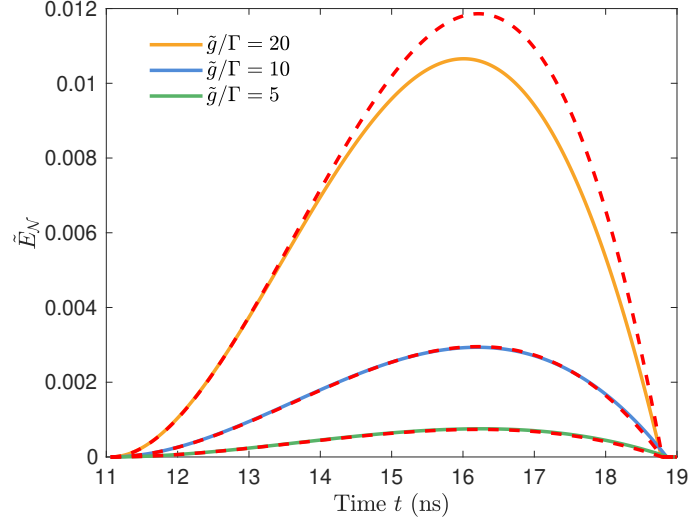


FIG. 8: (Color online) Time evolution of  $\tilde{E}_{\mathcal{N}}$  for different coupling strength at temperature 30 K, where solid curves denote the accurate simulation results and red dashed curves correspond to the approximated analytical results evaluated by Eq. (E25).

the main text, we assume that the initial time of the entanglement readout process is at  $\tau_1 + \tau_d$ , i.e.,  $t \in [0, \tau_1 + \tau_d]$ , thus Eq. (E25) can be rewritten as follows

$$\tilde{\lambda}_- \approx \frac{1}{2} \left[ 1 - \eta^2 t^2 + \frac{2}{3} \tilde{g}^2(\Gamma n_{\text{th}}) t^3 \right]. \quad (\text{E27})$$